Journal of Molecular Spectroscopy 327 (2016) 209–231

Contents lists available at ScienceDirect

Journal of Molecular Spectroscopy

journal homepage: www.elsevier.com/locate/jms

Oxygen dayglow emissions as proxies for atomic oxygen and ozone in the mesosphere and lower thermosphere

Valentine A. Yankovsky [a,*], Kseniia V. Martyshenko [a], Rada O. Manuilova [a], Artem G. Feofilov [b]

[a] St. Petersburg State University, 7/9 Universitetskaya nab., St. Petersburg 199034, Russia
[b] Laboratoire de Météorilogie Dynamique/IPSL/FX-Conseil, CNRS, Ecole Polytechnique, Université Paris-Saclay, 91128 Palaiseau, France

ARTICLE INFO

Article history:
Received 14 December 2015
In revised form 26 February 2016
Accepted 9 March 2016
Available online 11 March 2016

Keywords:
Ozone
Atomic oxygen
Remote sensing
Proxy
Molecular oxygen emissions
Mesosphere thermosphere

ABSTRACT

The main goal of this study is to propose and then to justify a set of methods for retrieving the [O] and [O_3] altitude distributions from the observation of emissions of the excited oxygen molecules and O(^{1}D) atom at daytime in the mesosphere and lower thermosphere (MLT) region. In other words, we propose retrieving the [O] and [O_3] using the proxies. One of the main requirements for the proxy is that the measured value should be directly related to a variable of our interest while, at the same time, the influence of the proxies on [O_3] and [O(^{3}P)] should be minimal. For a comprehensive analysis of different O_3 and O(^{3}P) proxies, we use a full model of electronic vibrational kinetics of excited products of O_3 and O_2 photolysis in the MLT of the Earth. Based on this model, we have tested five excited components; namely, $O_2(b^1\Sigma_g^+, v=0,1,2)$, $O_2(a^1\Delta_g, v=0)$ and O(^{1}D) as the [O_3] and [O(^{3}P)] proxies in the MLT region. Using an analytical approach to sensitivity studies and uncertainty analysis, we have therefore developed the following methods of [O(^{3}P)] and [O_3] retrieval, which utilise electronic-vibrational transitions from the oxygen molecule second singlet level ($O_2(b^1\Sigma_g^+, v=0,1,2)$. We conclude that $O_2(b^1\Sigma_g^+, v=2)$ and $O_2(b^1\Sigma_g^+, v=0)$ are preferable proxies for [O(^{3}P)] retrieval in the altitude range of 90–140 km, while $O_2(b^1\Sigma_g^+, v=1)$ is the best proxy for [O_3] retrieval in the altitude range of 50–98 km.

1. Introduction

The Earth's mesosphere and lower thermosphere (MLT) is important for its physical and chemical processes. Compared to the troposphere, this region is less accessible to observations, while its study is important for the following reasons: (1) the MLT area acts as a gateway between Earth and space, absorbing solar radiance in a number of bands in the region of 200–600 nm [1] and cooling the atmosphere in CO_2, O_3 and H_2O infrared bands (e.g. [2]); (2) the MLT area is considered to be an indicator of greenhouse gas changes and dynamics in the lower atmosphere; (3) most of the infrared satellite observations of the lower atmosphere, both in limb and even in nadir mode, are sensitive to the contribution of the MLT.

Ozone and atomic oxygen are the key components of the middle atmosphere influencing the composition and energy budget of this region in a large number of ways. In particular, atomic O concentration defines the infrared cooling of the MLT [3,4], affecting both the temperature and height of the mesopause; that is, the stronger the cooling, the colder and higher the mesopause [5].

A comprehensive review of the [O_3] measurement methods is presented in [6]. Currently, the accepted methods for remote sensing of altitude profile of the [O(^{3}P)] in the MLT are the measurements of excited O(^{1}S) green line emission intensity above approximately 90 km and the OH(v', v'') bands intensity measurements below 95 km height, only for the nighttime [7]. For daytime, there are no reliable methods for the remote sensing of the [O(^{3}P)] altitude profile in the MLT [7].

In this study, we set out and justify the methods we set out for retrieving the [O] and [O_3] vertical distributions from the observation of emissions of the electronically–vibrationally excited oxygen molecules and O(^{1}D) atom. In other words, we propose using the proxies to retrieve the [O] and [O_3]. One of the main requirements for the proxy is that the measured value should be directly related to a variable of our interest while, at the same time, the influence of the proxies on [O_3] and [O(^{3}P)] should be minimal.

We have to stress that we are looking for the indirect methods of the [O(^{3}P)] retrieval independently from [O_3] retrieval and vice versa. For this, we introduce a concept of proxies based on our extended photochemical model. The proxies we suggest are

* Corresponding author.
E-mail addresses: vyankovsky@gmail.com, valentine.yankovsky@spbu.ru (V.A. Yankovsky), ocsi18@mail.ru (K.V. Martyshenko), r.manuylova@spbu.ru (R.O. Manuilova), artem.feofilov@lmd.polytechnique.fr (A.G. Feofilov).

http://dx.doi.org/10.1016/j.jms.2016.03.006
0022-2852/

supposed to allow tracking fast variations of ozone and atomic oxygen concentrations (with characteristic periods from one to tens of minutes) associated with atmospheric dynamics, solar spectrum changes, and so on. Knowing the proxies, one can retrieve $[O(^3P)]$ and $[O_3]$ from the emissions of electronically–vibrationally excited O_2 molecules in the visible and near infra-red spectral region.

The main goal of this study is to identify the optimal proxies for $[O_3]$ and $[O(^3P)]$ retrieval at daytime in the MLT region. For a comprehensive analysis of these proxies, we use a full model of electronic vibrational kinetics of excited products of O_3 and O_2 photolysis in the MLT of the Earth (hereafter, YM2011) [8,9]. Here, the traditional kinetics of electronically excited products of O_3 and O_2 photolysis is supplemented with the processes of energy transfer among electronically–vibrationally excited levels $O_2(a^1\Delta_g, v)$ and $O_2(b^1\Sigma_g^+, v)$, excited atomic oxygen $O(^1D)$, and the O_2 molecules in the ground electronic state $O_2(X^3\Sigma_g^-, v)$.

Based on the YM2011 model, we tested 5 excited components: $O_2(b^1\Sigma_g^+, v = 0,1,2)$, $O_2(a^1\Delta_g, v = 0)$ and $O(^1D)$ as the proxies of $[O_3]$ and $[O(^3P)]$ in the MLT region. Generally speaking, each considered excited level could be a proxy of $[O_3]$ and/or $[O(^3P)]$, being that each of these 5 excited components depends on O_3 and/or $O(^3P)$ both in production and in quenching.

The structure of the work is as follows. In Section 2 we present a system of electronic and vibrational levels used in the YM2011 model, which will prove necessary to our discussion. We consider all the significant aeronomical reactions of photoexcitation, radiative quenching and energy transfer processes at collisions with $O(^3P)$, O_2, N_2, O_3 and CO_2. For collisional reactions, all the possible processes of energy transfer between excited levels have been taken into account, while Appendix A contains an overview of currently available kinetic data. Section 3 is an overview of the methods of $[O(^3P)]$ and $[O_3]$ retrieval in the MLT.

In Section 4, in the framework of YM2011 model we present the solution of forward problem for every proxy at each altitude, providing the differential kinetic equations for the afore-mentioned excited components in Appendix B. In Section 5, we show the sensitivity of five potential proxies to $[O_3]$ and $[O(^3P)]$ and to the other parameters of the model. We also provide the results of the sensitivity study for the inverse problem – the $[O_3]$ and $[O(^3P)]$ retrieval – to proxy concentrations and other parameters of the model. In association with this section, Appendix C contains the analytical formulae for sensitivity coefficients of solutions of forward and inverse problems ($[O(^3P)]$ and $[O_3]$ retrieval) – using, for example, $[O_2(b^1\Sigma_g^+, v = 1)]$ as a proxy – to all parameters included in the kinetic equation for $[O_2(b^1\Sigma_g^+, v = 1)]$.

In Sections 6 and 7 respectively, we present the estimates of photochemical lifetimes and volume emission rates (VER) for each proxy in the MLT. In Section 8, we consider the whole complex of aeronomical reactions influenced on $[O(^3P)]$ and $[O_3]$ altitude profiles retrieval (Section 8.1). Moreover, in Section 8.2 we discuss the choice of the optimal methods of $[O(^3P)]$ and $[O_3]$ retrieval for different altitude ranges. Here, we provide recommendations to the community on choosing/using the proxies and explain the optimal altitude intervals for $[O_3]$ and $[O(^3P)]$ retrieval from these proxies. In Section 8.3 we present the analytical formulae for $[O_3]$ and $[O(^3P)]$ retrieval using one of the suggested proxies; namely, $O_2(b^1\Sigma_g^+, v = 1)$. In Section 9, we give the main conclusions of the study and, in summarising our research, provide recommendations for the practical realisation of $[O_3]$ and $[O(^3P)]$ altitude distribution remote sensing in MLT.

We would like to summarise briefly the new investigations and results of this study:

1. We have used the comprehensive model of electronic-vibrationally kinetics of the electronically–vibrationally excited oxygen molecules and atom $O(^1D)$, (YM2011) for the first time, in order to find possible O_3 and $O(^3P)$ proxies amongst these excited components.
2. We have compiled the experimental data on the rate coefficients of energy transfer processes among electronically–vibrationally excited levels of O_2 molecule, as well as quantum yields of the products of these processes, with the measured errors of these factors. In so doing, we have created the database for more than 60 reactions.
3. The model of kinetics YM2011 and the database of experimental data both enable us to work out the analytical methods of sensitivity study and uncertainty analysis for all proposed proxies.
4. These methods, in turn, enable us to work out a new approach to $[O_3]$ and $[O(^3P)]$ retrieval. In short, $O_2(b^1\Sigma_g^+, v = 1)$ is the preferable proxy for the whole altitude range 50–100 km for O_3; for $[O(^3P)]$ retrieval $O_2(b^1\Sigma_g^+, v = 2)$ is the best proxy in the 90–140 km and the possible proxies above 95 km are $O_2(b^1\Sigma_g^+, v = 0)$ and $O_2(b^1\Sigma_g^+, v = 1)$.
5. In the altitude range of 90–105 km, we have worked out a method of $[O_3]$ and $[O(^3P)]$ altitude profiles simultaneous retrieval, which requires using both of the two proxies.
6. We have determined the restrictions inherent to traditional methods of $[O_3]$ retrieval from emissions at 1.27 μm and 762 nm. These could not be made without inclusion in the model of vibrational kinetics.
7. The sensitivity study has enabled us to obtain the approximate analytical formulae for $[O_3]$ and $[O(^3P)]$ retrieval using proxies $O_2(b^1\Sigma_g^+, v = 1)$.

2. Model of electronic-vibrational kinetics of the excited products of the O_2 and O_3 photodissociation in the MLT

2.1. Levels and transitions

Usually, the development of any complex kinetic model passes through a number of iterations and updates. The model of electronic-vibrational kinetics of the O_2 and O_3 photodissociation products in the MLT is not an exception. Initially, the exploratory variant was presented in [10], while the detailed description of the operative model was given in [1] (YM2006 model), which considered the populations of 35 electronic-vibrational excited states of the O_2 molecule and of atomic oxygen $O(^1D)$. In this model, we also took into account the photolysis of O_2 in the Schumann–Runge continuum and Lyman-α H atom and of O_3 in the Hartley band.

In the new extended YM2011 model of O_2 and O_3 photodissociation in the MLT, the kinetic balance equations were considered for 45 levels: three electronic-vibrationally excited levels $O_2(b^1\Sigma_g^+, v \leqslant 2)$, six levels $O_2(a^1\Delta_g, v \leqslant 5)$, 35 levels $O_2(X^3\Sigma_g^-, v \leqslant 35)$ and level $O(^1D)$ [8,9]. Besides the O_3 photolysis in spectral Hartley band, we also considered the photolysis in the Chappuis, Huggins and Wulf spectral bands in the interval of 200–900 nm. These channels give rise to the $O_2(X^3\Sigma_g^-, v = 1–35)$ vibrational levels of ground electronic state, which are then depopulated by V–V and V–T (vibrational–translational) energy exchange processes in collisions with O_2, N_2, $O(^3P)$, O_3 and CO_2 molecules. The populations of all 45 states are described by the system of kinetic balance equations. Hence, in YM 2011, we have developed the method to solve it.

In this study, we focus on the part of YM2011 kinetic model that describes the kinetics of 10 excited levels: $O(^1D)$, 3 levels $O_2(b^1\Sigma_g^+, v \leqslant 2)$ and 6 levels $O_2(a^1\Delta_g, v \leqslant 5)$ (Fig. 1). We will exclude the $O_2(X^3\Sigma_g^-, v = 0–35)$ levels from the consideration because their populations do not influence those of $O_2(a^1\Delta_g, v = 0–5)$ and $O_2(b^1\Sigma_g^+, v = 0,1,2)$. The O_2 photolysis in the Schumann–Runge continuum leads to the formation of two oxygen atoms: one in the ground electronic state $O(^3P)$ and the other one in the excited electronic state $O(^1D)$. Ozone photolysis in the Hartley band also leads to the formation of the $O(^1D)$ atom and of the O_2 molecule in the first electronic excited state $O_2(a^1\Delta_g, v = 0–5)$ in a singlet channel.

Since the beginning of the 1980s, laboratory data has shown that quantum yields of the $O_2(a^1\Delta_g, v = 0–5)$ production by O_3 photolysis in the Hartley band $F(HB \rightarrow O_2(a^1\Delta_g, v))$ strongly depend on the wavelength of photolytic radiation. For this study, we have used analytical expressions for quantum yields of electronically–vibrationally excited $O_2(a^1\Delta_g, v = 0–5)$ molecules depending on the wavelength and vibrational number for the entire Hartley band, described in detail in [11,12].

Collisional quenching of $O(^1D)$ atomic state by O_2 produces the $O_2(b^1\Sigma_g^+, v = 0, 1)$ excited electronic states. The main channel (quantum yield of approximately 0.8) corresponds to the $O_2(b^1\Sigma_g^+, v = 1)$ excitation. Besides collisional processes, the solar radiance absorption in the 762 nm (g_α), 688 nm (g_β) and 629 nm (g_γ) bands populates the $O_2(b^1\Sigma_g^+, v = 0)$, $O_2(b^1\Sigma_g^+, v = 1)$, and $O_2(b^1\Sigma_g^+, v = 2)$ states, respectively. In the collisional processes, the energy is then transferred from $O_2(b^1\Sigma_g^+, v = 0)$ to $O_2(a^1\Delta_g, v = 0–3)$. An additional source of $O_2(a^1\Delta_g, v = 0)$ population is the absorption of solar radiation by O_2 molecules in the 1.27 μm band (g_{IRa}).

The methodology developed in YM2011 permits one to solve the system of 10 kinetic equations for populations of electronically–vibrationally excited levels of oxygen molecule $O_2(a^1\Delta_g, v = 0–5)$, $O_2(b^1\Sigma_g^+, v = 0,1,2)$ and excited oxygen atom $O(^1D)$. Overall, the model includes more than 60 aeronomical reactions of photoexcitation and de-excitation, of energy transfers between these excited levels, and describes the quenching of the levels in collisions with $O(^3P)$, O_2, N_2, O_3 and CO_2 molecules. The corresponding rate coefficients and quantum yields are presented in Appendix A, in which we perform a comprehensive survey of currently available experimental data. In Appendix B, we provide differential kinetic equations for the $O(^1D)$, $O_2(b^1\Sigma_g^+, v = 0,1,2)$ and $O_2(a^1\Delta_g, v = 0–5)$ levels.

2.2. Reactions rate coefficients

In accordance with the scheme in Fig. 1, we consider more than 60 aeronomical reactions of photoexcitation, radiative and collisional processes (see Appendices A and B). For the latter, the reviews available of the chemical kinetics data [13,14] do not contain kinetic data on energy transfer reactions of the oxygen molecule electronically–vibrationally excited states with vibrational quantum number $v \geqslant 1$. In fact, the most important rate coefficients have been measured or estimated by different laboratory methods for several reactions of quenching: $O_2(b^1\Sigma_g^+, v = 1) + M\,(O_2, O(^3P)) \rightarrow$ *products* [15–18], $O_2(b^1\Sigma_g^+, v = 1 \text{ and } 2) + O_2 \rightarrow$ *products* [19], $O_2(a^1\Delta_g, v = 1) + M(O_2 \text{ or } O_3) \rightarrow$ *products* [20–23], $O_2(A^3\Sigma_u^+, v = 0–4) + M\ (O_2, N_2, O_2(a^1\Delta_g, v = 0), CO_2, O(^3P), Ar) \rightarrow$ *products* and $O_2(c^1\Sigma_g^+, v = 0) +$

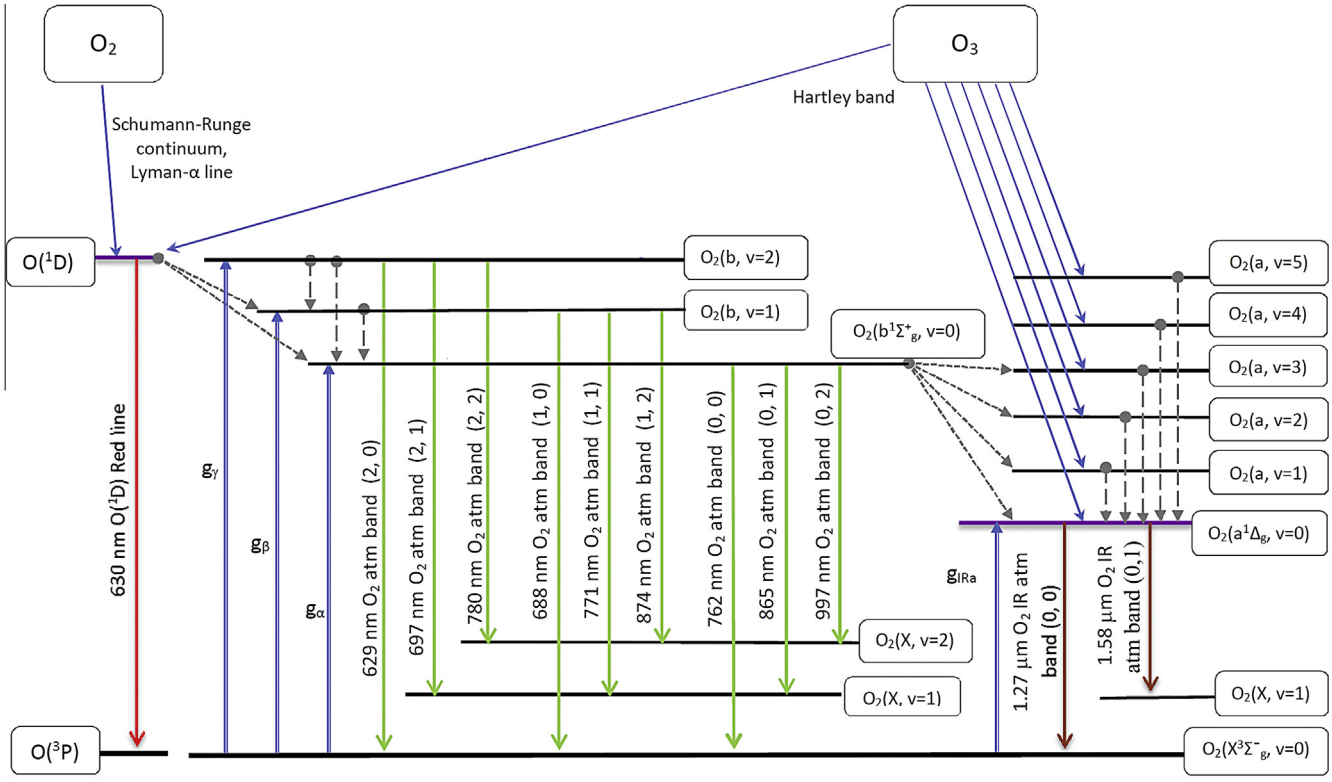

Fig. 1. Scheme of kinetics of 10 excited levels, based on the YM2011 model: $O(^1D)$, three $O_2(b^1\Sigma_g^+, v = 0–2)$ levels, and six $O_2(a^1\Delta_g, v = 0–5)$ levels. Solid lines with arrows designate the processes of O_2 and O_3 photolysis. Double vertical lines with the arrows pointed upwards designate the processes of solar radiation absorption in the 762 nm (g_α), 688 nm (g_β), 629 nm (g_γ) and in the 1.27 μm (g_{IRa}) bands. Dotted lines with arrows present energy transfer from $O(^1D)$ to the $O_2(b^1\Sigma_g^+, v = 0, 1)$ and from $O_2(b^1\Sigma_g^+, v = 0)$ to $O_2(a^1\Delta_g, v = 0–3)$ at collisional quenching. Dashed vertical lines with arrows pointed down stand for collisional V–V transitions. Solid vertical lines with arrows pointed down designate the processes of radiative emissions from electronic-vibrational levels of O_2 molecule and from excited atom $O(^1D)$.

M (O_2, N_2, $O_2(a^1\Delta_g, v=0)$, CO_2, $O(^3P)$, Ar) → *products* [24,25], $O_2(b^1\Sigma_g^+, v=2) + O_2$ → *products* [26].

A large discrepancy between the rate coefficients values obtained by different methods had led to a natural scepticism about the accuracy of these measurements [27]. The breakthrough in this field is associated with the works of Hwang et al. [28] and Slanger and Copeland [29], who managed to measure the rate coefficients of the $O_2(b^1\Sigma_g^+, v=1,2,3)$ and $O_2(a^1\Delta_g, v=1)$ quenching in collisions with different partners. A peculiarity of the electronic–electronic (E–E) energy transfer is that the vibrational excitation quantum number is conserved:

$$O_2(b^1\Sigma_g^+, v) + O_2(X^3\Sigma_g^-, v'=0) \rightarrow O_2(X^3\Sigma_g^-, v) + O_2(b^1\Sigma_g^+, v'=0) \quad (1)$$

while this reaction is 2–3 order of magnitude faster than the reactions of vibrational quanta exchange (V–V) within the same electronic state:

$$O_2(b^1\Sigma_g^+, v) + O_2(X^3\Sigma_g^-, v'=0) \rightarrow O_2(b^1\Sigma_g^+, v=0) + O_2(X^3\Sigma_g^-, v'=v) \quad (2)$$

The same is true for the similar reaction with $O_2(a^1\Delta_g, v)$. The first generalised review of the afore-mentioned studies [28,29,21,26] and also [30,31] was presented in [1] within the framework of the YM2006 model development. Therefore, we present in this study the first systematic review of contemporary available kinetic data up to 2015 (see Appendix A).

3. Atomic O and O_3 remote sensing in the MLT: current status

The remote sensing of atomic $O(^3P)$ concentrations in the MLT has been in development since the early 1970s. We list below the observation approaches that are currently known:

(a) Rocket-borne experiments using the resonance fluorescence method measuring the intensity of the $O(^3S–^3P)$ transition at 130 nm ([32] and references therein). When using this method, it should be noted that the absolute densities retrieved in the same area are not always consistent. This may be a sign of large experimental uncertainties [32].
(b) Atomic $O(^3P)$ retrieval from the fine structure of 63 μm spectral line corresponding to the $O(^3P_1–^3P_2)$ transition suggested in [33] was realised in the CRISTA-1 (November 1994) and CRISTA-2 (August 1997) experiments [34] in the 130–175 km altitude range using the MSIS thermospheric temperatures in the retrievals. The values obtained for the altitudes of CRISTA measurements were about 40% lower than those predicted by the MSIS model for the low solar activity conditions of the experiment [35].
(c) The measurements of excited $O(^1S)$ green line emission intensity above approximately 90 km (nighttime).
(d) The OH(v', v'') bands intensity measurements below 95 km (nighttime).
(e) The results obtained by methods (c) and (d) demonstrate quite a large spread [32,36,37].

Besides these methods, some new $[O(^3P)]$ retrieval approaches have been suggested but have not yet been realised:

(a) In 1991, based on the O_2 glow discharge experiment [30], Yankovsky suggested using the 771 nm Atmospheric band (1,1) emission corresponding to the $O_2(b^1\Sigma_g^+, v=1) \rightarrow O_2(X^3\Sigma_g^-, v=1)$ transition as an $O(^3P)$ proxy for the daytime MLT. In 2012, Yee et al. [38] also suggested to retrieve $[O(^3P)]$ from the emissions of $O_2(b^1\Sigma_g^+, v=1)$ molecules. The list of reactions considered in [38] is the same as in [1], excluding the processes of excitation and quenching of the $O_2(b^1\Sigma_g^+, v=2)$ level and its interaction with the lower levels. It is worth noting that the attempts of Yee et al. [38] to consider the $O_2(b^1\Sigma_g^+, v=1)$ kinetics above 140 km up to 250 km, have forced them to use the reaction coefficients measured at room temperatures for a temperature up to 1000 K.
(b) In 2006, Slanger [39] suggested the $O(^1D)$ as a daytime proxy of $[O(^3P)]$ in the thermosphere above 150 km.
(c) In 2009, Hedin et al. [32] suggested a method of using $O_2(b^1\Sigma_g^+, v=0)$ nighttime emission in an O_2 Atmospheric band (0,0) for the $[O(^3P)]$ retrieval.
(d) In 2011, Yankovsky et al. [40] considered the possibilities of $[O(^3P)]$ and $[O_3]$ retrieval from daytime emissions formed by the transitions from $O_2(b^1\Sigma_g^+, v=0,1,2)$ levels, populated as a result of O_3 and O_2 photolysis.

For the altitude region of 65–105 km, Mlynczak et al. [7] have obtained day and night atomic oxygen altitude profiles based on SABER-TIMED data. The nighttime atomic oxygen profiles have been retrieved from an observed OH emission. The daytime atomic oxygen concentration profiles were derived from $[O_3]$ altitude profiles retrieved from the measured radiation in 9.6 μm O_3 band using the steady state equation for the three-body O_3 recombination and O_3 photolysis in the Hartley band.

A comprehensive review of $[O_3]$ measurement methods [6] serves to analyse the discrepancies between several experiments, such as HALOE, HRDI, MIPAS, GOMOS, ACE-FTS, SOFIE, OSIRIS, SMILES and TIMED-SABER. In their analysis, Smith et al. [6] noticed that daytime ozone concentrations retrieved from the 9.6 μm channel of SABER is 20–50% higher in the interval of 60–80 km than that derived from the other measurements. The difficulties of ozone concentrations retrieval from the observation of emission in 9.6 μm band is explained by the complexity of the vibrational kinetics of O_3 molecule [41,2]. The methods under discussion – namely, the measurements of airglow emission in 762 nm Atmospheric band (0,0) and in 1.27 μm IR Atmospheric band (0,0) – are so utilised by HRDI, OSIRIS, SABER. For the interpretation of these experiments, they used a model of pure electronic kinetics developed by Mlynczak et al. [42].

4. Forward problem: proxy level populations

The generalised form of differential kinetic nonlinear equations for population of i-th excited level n_i from Appendix B (see formulae (1–10) in Table B1) is:

$$\frac{\partial n_i}{\partial t} = \sum_{k=1;k\neq i}^{10} n_k \cdot p_i^k + \sum_l F_i^l - n_i \cdot \left(\sum_r A_i^r + \sum_m q_i^m \right) \quad (3)$$

where p_i^k is the production rate for the i-th excited component related to the energy transfer at collisions with the k-th component (if such transfer is impossible, then $p_i^k = 0$); F_i^l is the production rate for the i-th component at l-th process of O_2, O_3 photodissociation or chemical reaction. The terms in the parenthesis in (3) represent a quenching factor for level n_i, where A_i^r are Einstein coefficients of radiative deactivation to all lower levels and q_i^m is the quenching rate of the i-th component due to collisional deactivation in the m-th process. The values of the rate coefficients, the quantum yields of excited products and the Einstein coefficients are in Tables 7.1, A1 and B2.

The system of Eq. (3) can be written in the form of the matrix equation for the vector of the state populations **n**

$$\partial \mathbf{n}/\partial t = \mathbf{An} + \mathbf{F} \quad (4)$$

where **A** matrix describes the energy transfer processes among the excited levels under consideration. This matrix is quasi-diagonal and strongly sparse; only about 30% of its elements are greater than zero [1].

For the problems considered in this study, we use a stationary case of Eq. (4):

$$\mathbf{n} = -\mathbf{A}^{-1}\mathbf{F} \quad (5)$$

For all the components considered, we have obtained analytical solutions for the stationary equations system. This allows us to calculate simultaneously the altitude profiles of concentrations of molecules $O_2(a^1\Delta_g, v = 0–5)$, $O_2(b^1\Sigma_g^+, v = 0,1,2)$ and of excited oxygen atom $O(^1D)$. However, for the comprehensive analysis of potential proxies, we have used the YM2011 model to test the 5 excited components – namely, $O_2(b^1\Sigma_g^+, v = 0,1,2)$, $O_2(a^1\Delta_g, v = 0)$ and $O(^1D)$ – while the remaining five of ten components, $O_2(a^1\Delta_g, v = 1–5)$ are not to be taken as proxies because their population are three orders of magnitude smaller than the other ones [1].

To illustrate the method involved here, we present the altitude profiles of the $O_2(b^1\Sigma_g^+, v = 0,1,2)$ daytime concentrations for 150 TIMED-SABER events of the autumn equinox of 2010 (Fig. 2). For the calculation of the photodissociation and photoexcitation rates, we have used the corresponding SORCE solar irradiance data [43]. The atmospheric composition and the altitude profiles of kinetic temperature were taken from the SABER retrievals (V2.0, http://saber.gats-Inc.com/data.php) [44].

As can be seen in Fig. 2, the altitude distributions of the $[O_2(b^1\Sigma_g^+, v = 1)]$ and $[O_2(b^1\Sigma_g^+, v = 2)]$ are different. The former has a minimum at ~80 km while the latter has a maximum around this height. Above 90 km, the $[O_2(b^1\Sigma_g^+, v = 1)]$ is relatively stable while the $[O_2(b^1\Sigma_g^+, v = 2)]$ decreases; both profiles do not strongly depend on latitude or solar zenith angle (SZA). We would explain this observed behaviour by a combination of pumping/quenching processes (Appendix A) and their altitude changes.

5. Sensitivity study

To compare the characteristics of the assumed proxies, we have performed a sensitivity analysis of the forward calculations of concentrations of all the proxies to all the parameters of the YM2011 model (more than 60). We have tested the supposed proxies in the altitude range of 50–140 km for different solar zenith angles (SZA) and latitudes using a set of atmospheric profiles retrieved from SABER measurements.

We then carried out the comparative analysis of sensitivity of all proxies to $[O_3]$ and $[O(^3P)]$.

5.1. Sensitivity analysis of the forward problem

Let's write the kinetic Eq. (3) in the following simplified form:

$$\frac{\partial x_m}{\partial t} = P_m(z_i) - x_m \cdot Q_m(z_i), \quad (6)$$

where x_m is the concentration of excited molecules of $O_2(b^1\Sigma_g^+, v = 0–2)$, $O_2(a^1\Delta_g, v = 0–5)$ and the atom $O(^1D)$ (in cm^{-3}); z_i are parameters of the model (e.g., the main atmospheric component concentrations, the rates of photoprocesses, the reaction rate coefficients, the quantum yields of the reaction products and so forth.); $P_m(z_i)$ is the production rate of the component x_m (in $cm^{-3}\ s^{-1}$), $Q_m(z_i)$ is a factor of quenching of the component x_m in the radiative and collisional processes (see formula (B.1)).

The total differential of the calculated values x_m depends on the partial derivatives with respect to all the parameters of the model. The dimensionless value of $\frac{dx_m}{x_m}$, where dx_m is the total differential of x_m, depends on the relative variations of all the model parameters, $\frac{dz_i}{z_i}$:

$$\frac{dx_m}{x_m} = \sum_{i=1}^{n_z} S(x_m; z_i) \cdot \frac{dz_i}{z_i} \quad (7)$$

where n_z is the total number of variable parameters in Eq. (6) and $S(x_m; z_i)$ is called the sensitivity coefficient of the target function x_m to variation of parameter z_i:

$$S(x_m; z_i) = \frac{z_i}{x_m} \cdot \frac{\partial x_m}{\partial z_i} \quad (8)$$

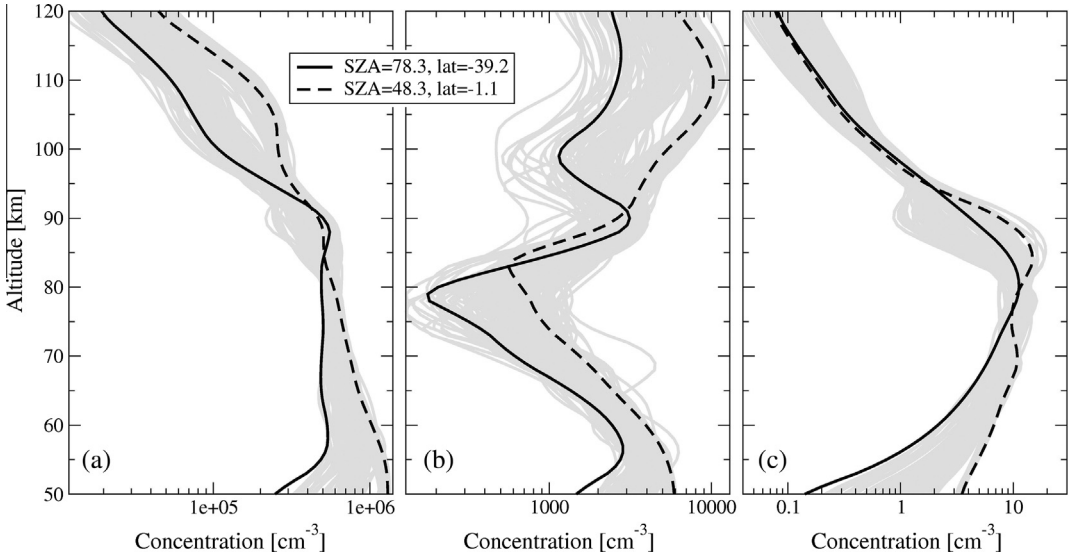

Fig. 2. Altitude profiles of $[O_2(b^1\Sigma_g^+, v = 0–2)]$ calculated for 150 TIMED-SABER events in autumn equinox 2010 (Day = 265, 2010; latitudes from −43.8° to 75.0°; SZA from 46.0° to 82.0°): (a) $[O_2(b^1\Sigma_g^+, v = 0)]$, (b)$[O_2(b^1\Sigma_g^+, v = 1)]$, (c) $[O_2(b^1\Sigma_g^+, v = 2)]$. To show the dependence of $[O_2(b^1\Sigma_g^+, v = 0–2)]$ on latitude and solar zenith angle, solid and dashed curves mark the profiles of two strongly different events.

The numerical estimates of the sensitivity coefficients, $S(x_m; z_i)$, are often used instead of analytical expressions. They can be calculated numerically by perturbing the parameter around the base value. These estimates are usually made only for the fixed discrete values of variations $(\Delta z_i)/z_i = 0.05$ (occasionally, 0.01 or 0.1).

Meanwhile, from the kinetic Eq. (6) in the stationary case, one can obtain the sensitivity coefficients in an analytical form simply by taking the partial derivatives with respect to all the parameters of the model. Obviously, the analytical expression enables one to calculate the sensitivity coefficients for every possible values of the parameter.

In Appendix C, in respect to the forward problem of calculation of the altitude profile of the metastable molecules $O_2(b^1\Sigma_g^+, v=1)$ concentration (Table C1), we present an example of analytical formulae for the coefficients of sensitivity to parameters of the model. The coefficients of sensitivity were obtained from the kinetic equation for the $O_2(b^1\Sigma_g^+, v=1)$ (formula 3 from Table B1), which becomes a balance equation in the case of quasi-stationary conditions in the 50–140 km altitude range:

$$[O_2] * g_\beta + [O(^1D)] \cdot [O_2] \cdot k(O(^1D); O_2) \cdot F(O(^1D) \to O_2(b, v=1); O_2) + \left[O_2\left(b^1\Sigma_g^+, v=2\right)\right] \cdot [O] \cdot k(O_2(b, v=2); O) \cdot F(O_2(b, v=2) \to O_2(b, v=1); O)) - \left[O_2\left(b^1\Sigma_g^+, v=1\right)\right] \cdot Q\left(O_2\left(b^1\Sigma_g^+, v=1\right)\right) = 0. \quad (9)$$

Similarly, we obtained the sets of sensitivity coefficients in analytical form to all the parameters of the YM2011 model, $S(proxy; z_i)$ and for all types of proxy proposed in this paper (using equations from Appendix B), excluding $O_2(a^1\Delta_g, v=0)$. For the latter, we only calculated the sensitivity coefficients numerically. For the sake of space, we will not present the same analytical formulae for the other proxies.

To improve the clarity of further analysis, we suggest the following gradation of sensitivity coefficients values in Table 5.1.

In Figs. 3–10 and 12 we present altitude profiles of sensitivity coefficients with normal or strong gradation values in correspondence with Table 5.1.

The results of sensitivity study of the forward problem for proxies $O(^1D)$, $O_2(b^1\Sigma_g^+, v=2)$, $O_2(b^1\Sigma_g^+, v=1)$, $O_2(b^1\Sigma_g^+, v=0)$ and $O_2(a^1\Delta_g, v=0)$ are presented in Figs. 3–7, respectively.

It should be emphasised that, in Figs. 3–14, we present calculations for the typical atmospheric conditions (SABER L2, 2010, day 172, latitude 43.0, SZA = 70.5, F10.7 = 74).

As one can see in Fig. 3, $[O(^1D)]$ is sensitive to $[O_3]$ only below 100 km, and to [O] above 105 km. An important particularity of this dependence is the sensitivity coefficient of $[O(^1D)]$ to a rate coefficient of reaction $O(^1D) + O_3 \to 2O_2$; namely, to $S(O(^1D); k(O(^1D); O_3))$ is less than 10^{-4} in the whole altitude range.

As observed in Fig. 4, $[O_2(b^1\Sigma_g^+, v=2)]$ is not sensitive to $[O_3]$ in the whole altitude range, but it is sensitive to [O] above 85 km, while $S(O_2(b^1\Sigma_g^+, v=2)); O(^3P))$ is close to -1, meaning that $[O_2(b^1\Sigma_g^+, v=2)]$ is inversely proportional to $[O(^3P)]$. It should be noted that above 95 km, $[O_2(b^1\Sigma_g^+, v=2)]$ almost does not depend at all on atmospheric temperature because $S(O_2(b^1\Sigma_g^+, v=2); T)$ is close to zero.

Table 5.1
Schematic gradation of sensitivity coefficients values.

$S(x_m; z_i)$	The relationship between x_m and z_i
$\lvert S\rvert > 1$	Strong nonlinear relationship
$S \cong 1$	$x_m \propto z_i$
$S \cong -1$	$x_m \propto (z_i)^{-1}$
$1 > \lvert S\rvert > 0.1$	Normal relationship
$\lvert S\rvert < 0.1$	Weak relationship

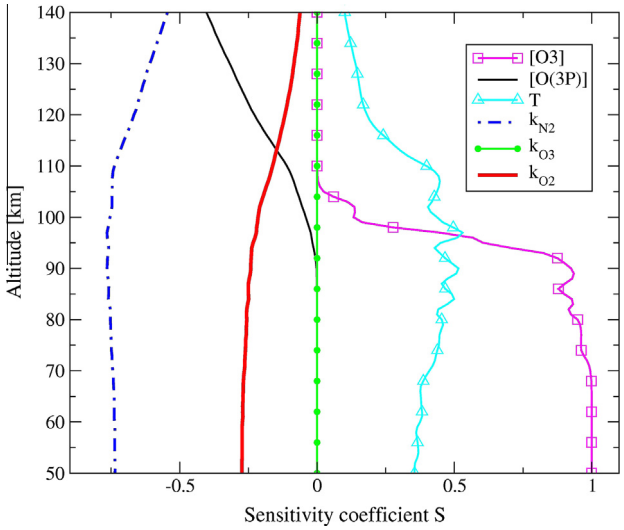

Fig. 3. Sensitivity coefficients, $S(O(^1D); parameter)$, for the forward problem where parameters are: $[O(^3P)]$ (thin solid line); $[O_3]$ (solid line with unfilled squares); atmospheric temperature (solid line with unfilled triangles); rate coefficients of quenching processes at collisions with N_2 (dashed-dotted line), O_3 (solid line with filled circles), O_2 (bold solid line).

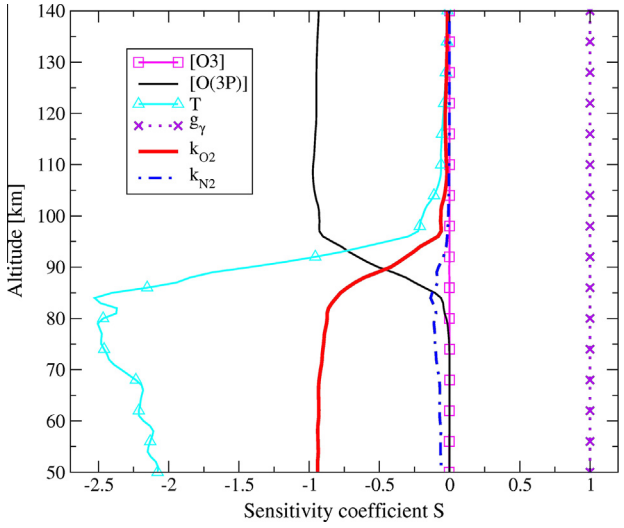

Fig. 4. Sensitivity coefficients, $S(O_2(b^1\Sigma_g^+, v=2); parameter)$, for the forward problem where parameters are: rate of solar radiation absorption in 629 nm band, g_γ (dotted line with crosses). Sensitivity coefficients of $O_2(b^1\Sigma_g^+, v=2)$ to parameters $[O_3]$, $[O(^3P)]$, atmospheric temperature and rate coefficients of quenching processes at collisions with N_2, O_2 are marked the same way as in Fig. 3.

Fig. 5 shows that $[O_2(b^1\Sigma_g^+, v=1)]$ is sensitive to $[O_3]$ below 100 km, and $[O_2(b^1\Sigma_g^+, v=1)]$ is directly proportional to $[O_3]$ below 90 km. In addition, $[O_2(b^1\Sigma_g^+, v=1)]$ is sensitive to $[O(^3P)]$ above 95 km. The sensitivity coefficient to quantum yield of $O_2(b^1\Sigma_g^+, v=1)$ in reaction $O(^1D) + O_2 \to O_2(b^1\Sigma_g^+, v) + O(^3P)$ is close to 1 in the whole altitude range considered. In Appendix C, the analytical formulae for the sensitivity coefficients for $O_2(b^1\Sigma_g^+, v=1)$ include dependence on all parameters of the model.

Fig. 6 shows that $[O_2(b^1\Sigma_g^+, v=0)]$ is sensitive to $[O_3]$ below 100 km where $S(O_2(b^1\Sigma_g^+, v=0)); O_3)$ is about 0.4. Besides that,

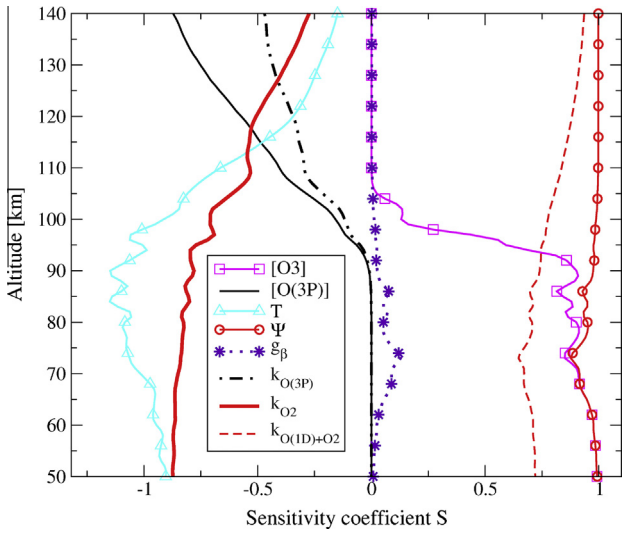

Fig. 5. Sensitivity coefficients, $S(O_2(b^1\Sigma_g^+, v=1); parameter)$, for the forward problem where parameters are: rate of solar radiation absorption in 688 nm band, g_{β} (dotted line with asters); rate coefficients of quenching processes of $O_2(b^1\Sigma_g^+, v=1)$ at collisions with $O(^3P)$ (double dotted-dashed line). The sensitivity coefficient of $O_2(b^1\Sigma_g^+, v=1)$ to the rate coefficient of reaction $O(^1D) + O_2 \rightarrow O_2(b^1\Sigma_g^+, v) + O(^3P)$ is marked by thin dashed line, and to quantum yield of $O_2(b^1\Sigma_g^+, v=1)$ in this reaction, ψ, is marked by line with unfilled circles. Sensitivity coefficients of $O_2(b^1\Sigma_g^+, v=1)$ to parameters $[O_3]$, $[O(^3P)]$, atmospheric temperature and rate coefficient of quenching process at collisions with O_2 are marked the same way as in Fig. 3.

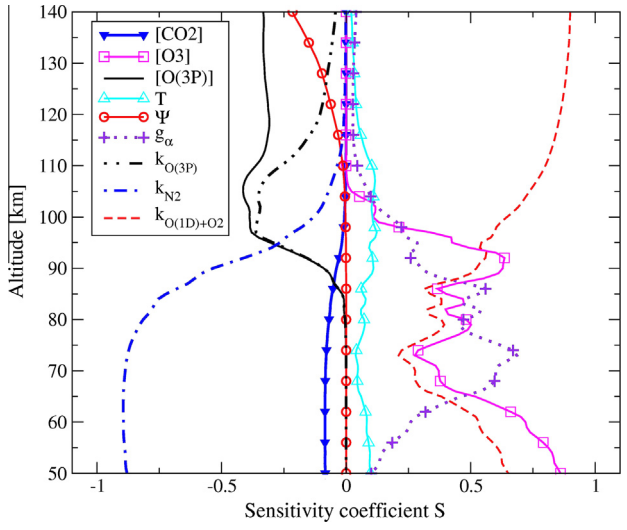

Fig. 6. Sensitivity coefficients, $S(O_2(b^1\Sigma_g^+, v=0); parameter)$, for the forward problem where parameters are: $[CO_2]$ (solid line with filled triangles); rate of solar radiation absorption in 762 nm band, g_{α} (dotted line with crosses). The sensitivity coefficient of $O_2(b^1\Sigma_g^+, v=0)$ to $[O_3]$, $[O(^3P)]$, atmospheric temperature, and to the rate coefficients of quenching processes at collisions with $O(^3P)$ and N_2 and of reaction $O(^1D) + O_2 \rightarrow O_2(b^1\Sigma_g^+, v) + O(^3P)$ and also to quantum yields, ψ, and are marked the same way as in Fig. 5.

in the altitude interval of 100–140 km, the value of sensitivity coefficient of $[O_2(b^1\Sigma_g^+, v=0)]$ to $[O(^3P)]$ reaches -0.5. The sensitivity coefficient to quantum yield $S(O_2(b^1\Sigma_g^+, v=0); F(O(^1D) \rightarrow O_2(b^1\Sigma_g^+, v=1)))$ is very low; not more than ± 0.1 in the whole altitude range. We also observed a weak dependence of $[O_2(b^1\Sigma_g^+, v=0)]$ on $[CO_2]$ in the altitude interval of 50–95 km.

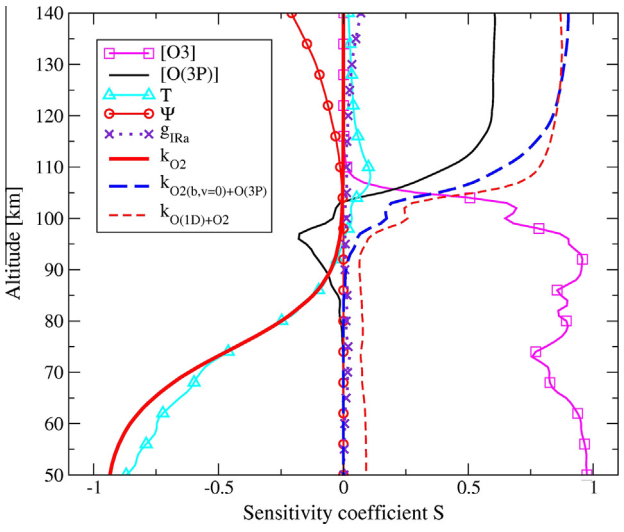

Fig. 7. Sensitivity coefficients, $S(O_2(a^1\Delta_g, v=0); parameter)$, for the forward problem where parameters are: rate of solar radiation absorption in 1.27 μm band, g_{IRa} (dotted line with crosses); rate coefficient of reaction $O_2(b^1\Sigma_g^+, v=0) + O(^3P) \rightarrow O_2(a^1\Delta_g, v=0) + O(^3P)$ (long dashed line). The sensitivity coefficient of $O_2(a^1\Delta_g, v=0)$ to $[O_3]$, $[O(^3P)]$, atmospheric temperature, and to the rate coefficients of quenching processes at collisions with O_2 and of reaction $O(^1D) + O_2 \rightarrow O_2(b^1\Sigma_g^+, v) + O(^3P)$ and also to quantum yields, ψ, and are marked the same way as in Fig. 5.

A well-known ozone proxy, $[O_2(a^1\Delta_g, v=0)]$ appears to be very sensitive to $[O_3]$ below 100 km (see Fig. 7). It is interesting to note that $[O_2(a^1\Delta_g, v=0)]$ depends on $[O(^3P)]$ above 115 km, where $S(O_2(a^1\Delta_g, v=0); O(^3P))$ is about 0.6.

Having summarised the results of the sensitivity analysis for all proxies (Figs. 3–7), in Fig. 8 we present the sensitivity coefficients to ozone for five proxies, $S(proxy; O_3)$. Here we see that $O_2(b^1\Sigma_g^+, v=1)$, $O_2(a^1\Delta_g, v=0)$ and $O(^1D)$ are potentially good O_3 proxies from 50 km and up to 100 km, with the values of $S(proxy; O_3)$ equal to 0.8–1.0. On the other hand, we cannot recommend using $O_2(b^1\Sigma_g^+, v=2)$ as the O_3 proxy because its sensitivity coefficients to $[O_3]$ are smaller than 0.05.

It may be seen from the sensitivity coefficients to atomic oxygen for the five proxies, $S(proxy; O(^3P))$, presented in Fig. 9, $O_2(b^1\Sigma_g^+, v=1)$ that $O_2(a^1\Delta_g, v=0)$ and $O(^1D)$ should not be used as $O(^3P)$ proxies below 110 km. The reason is that their sensitivity coefficients to $O(^3P)$ vary within ± 0.25 limits at these heights.

The best proxy is $O_2(b^1\Sigma_g^+, v=2)$ with the values of sensitivity coefficient $S(O_2(b^1\Sigma_g^+, v=2); O(^3P))$ close to -1 above 90 km. Meanwhile, $O_2(b^1\Sigma_g^+, v=0)$ are acceptable $[O(^3P)]$ proxies above 100 km.

5.2. Sensitivity analysis for the inverse problem

In most cases, an exact analytical solution of the inverse problem cannot be obtained due to the nonlinearity of the kinetic equations. In this study, the target functions of inverse problem are the $O(^3P)$ and O_3 concentrations. In comparison to the basic O_2, N_2, and CO_2 molecules, these atmospheric species can participate with greater efficiency in a variety of the formation and quenching processes of excited atmospheric components. In order to identify the key mechanisms for solving the inverse problem, we will thus carry out a complete analysis of the model's sensitivity to all the parameters.

There are two complementary analytical methods of calculating the sensitivity coefficients for the inverse problem:

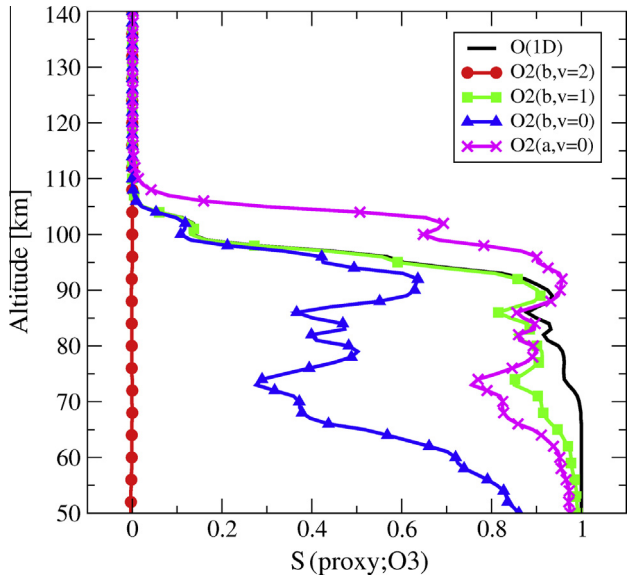

Fig. 8. Sensitivity coefficient for the forward problem, $S(proxy; O_3)$. Type of proxy: O (^{1}D) – solid line; $O_2(b^1\Sigma_g^+, v=2)$ – solid line with filled circles; $O_2(b^1\Sigma_g^+, v=1)$ – solid line with filled squares; $O_2(b^1\Sigma_g^+, v=0)$ – solid line with filled triangles; $O_2(a^1\Delta_g, v=0)$ – solid line with crosses.

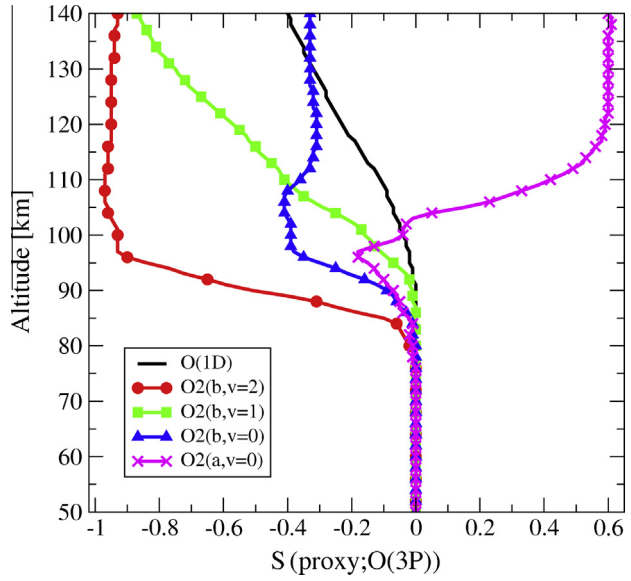

Fig. 9. Sensitivity coefficient for the forward problem, $S(proxy; O(^3P))$. See the type of proxy in the caption to Fig. 8.

(a) The direct derivation of the balance Eq. (6) for a stationary case; for example, (9) for $O_2(b^1\Sigma_g^+, v=1)$. This method is straightforward but, in some cases, it may lead to cumbersome formulae.

(b) Reduction method (using sensitivity coefficients of the forward problem).
Taking as a basis the known properties of partial derivatives for implicit function [45], we derive Eq. (10) from (6) in stationary conditions:

$$S_{x_k}(y_i; z_j) = -\frac{S(x_k; z_j)}{S(x_k; y_i)}, \tag{10}$$

where the left part of the expression (10) is the sensitivity coefficient of parameter y_i (e.g. O_3 or $O(^3P)$) to parameter z_j (rest parameters of the model) for the inverse problem, while the right part describes the ratio of the sensitivity coefficients for the forward problem; namely, term $-\frac{S(x_k;z_j)}{S(x_k;y_i)}$, where x_k is the proxy concentration.

An obvious consequence of (10) is the relationship between the sensitivity coefficients of the target functions and the parameters (for reasons of clarity, the indices have been omitted):

$$S(x; y) \cdot S(y; x) = 1 \tag{11}$$

Formula (11) states that the variable x is a 'good' proxy for target function y when the relationship between them is close to a direct or an inverse proportionality (id est. when the $|S(x; y)| \sim 1$, see Table 5.1).

Thus, the sensitivity coefficients $S(proxy; z_i)$ of the inverse problem could be derived for any proxy in the analytical form. However, the solution of the inverse problem is usually obtained numerically using kinetics equations from Appendix B.

In Appendix C, for the first time we present analytical formulae for the sensitivity coefficients $S(O_2(b^1\Sigma_g^+, v=1); parameter)$ for the forward problem (see Table C1) and also for the inverse problem $S(O_3; parameter)$ and $S(O(^3P); parameter)$ of the $[O_3]$ and $[O(^3P)]$ altitude profile retrieval, this time using $[O_2(b^1\Sigma_g^+, v=1)]$ as a proxy (see Tables C2 and C3, correspondingly). The sensitivity coefficients for all parameters of YM2011 model have been derived from (9) by straight differentiation or with the help of Reduction method (10).

The formulae were obtained in the same way for other proxies; we have therefore not presented them in order to save space. It should be noted, however, that the analytical formulae for the sensitivity coefficients include dependence on all parameters of the model.

5.3. Estimating the uncertainties of the forward and inverse problem solutions using sensitivity coefficients

Eq. (7) links the estimates of the forward (or inverse) problem solution uncertainty $\Delta x_m/x_m$ with known uncertainties of different parameters z_i of the YM2011 model. Instead of relative variations $\frac{dz_i}{z_i}$ we use the experimentally determined values of the relative errors of these parameters $\xi_i = \Delta z_i/z_i$. The values of rate coefficients and quantum yields, as well as the values of their absolute uncertainties, have been obtained from available experimental data (see Appendix A).

In general, all the parameters included in the model can be divided into three groups.

The external parameters:

(a) The altitude profiles of the main atmospheric components concentrations and of the atmospheric temperature are usually taken from reference databases (either a standard atmospheric model or, less commonly, direct experimental results).

(b) The altitude profiles of photoexcitation and photodissociation rates have been calculated taking into account the atmospheric composition, cross sections of the corresponding photoprocesses and the spectrum of solar radiance. The uncertainties of the photoprocess rates are not usually specified at the photochemical modelling stage. However, the uncertainties of the corresponding cross sections for O_2 and O_3 may range from a few to tens of percent depending on wavenumber range [46].
The internal parameters:

(c) There is currently an unambiguous association between the main source of uncertainty in the modelling of complex photochemical systems with errors in the rate coefficients and

the quantum yields of the products of the aeronomical reactions. The range of the relative errors of these parameters varies from four percent up to several hundred percent (see the experimentally determined values of ξ_i in Table A1 from Appendix A).

Each of these parameters (a, b, and c) has an independent effect on the uncertainty of the forward and/or the inverse problem solutions. Nonetheless, all these processes are coupled in the common photochemical model. The relative uncertainty of $\delta_m = \Delta x_m / x_m$ from (7) is connected with the sensitivity coefficients, $S(x_m; z_i)$, while the relative errors of all parameters are included, $\boldsymbol{\xi_i}$:

$$\delta_m = \sqrt{\sum_{i=1}^{n_z} (S(x_m; z_i))^2 \cdot (\xi_i)^2}, \quad (12)$$

Formula (12) is valid both for the forward and inverse problems. The same formula for absolute values of uncertainty of target function x_m, which depends on the relative uncertainties of parameters, z_i, has been obtained by von Clarmann (formula (9) from [47]). Previously, Chen et al. [48] used this formula to estimate the uncertainty of the forward problem.

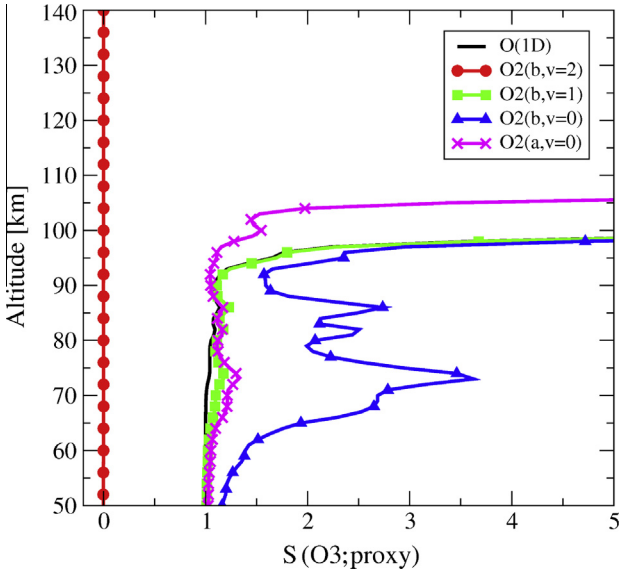

Fig. 10. Sensitivity coefficient, $S(O_3; proxy)$, for inverse problem of $[O_3]$ retrieval from proxy concentration. See the type of proxy in the caption to Fig. 8.

5.4. Ranking the proxies for $[O(^3P)]$ and $[O_3]$ retrieval

We rank the proxies based on two criteria. First, the altitude dependence of sensitivity coefficients for the inverse problem; and second, the altitude dependence of uncertainties of $[O(^3P)]$ and/or $[O_3]$ retrieval in correspondence with (12). In Figs. 10–11 and 12–13 we discuss the $[O_3]$ retrieval and the $[O(^3P)]$ retrieval respectively. Sensitivity coefficients of the inverse problem, $S(x_m; z_i)$, are then calculated numerically or analytically from (10) (as in Example for $O_2(b^1\Sigma_g^+, v=1)$ in Appendix C).

5.4.1. $[O_3]$ retrieval

We show the sensitivity coefficients $S(O_3; proxy)$ for the inverse problem in Fig. 10. In accordance with (11), the absolute values of sensitivity coefficients for the 'good' proxy should be close to 1. As one can see in Fig. 10, three proxies ($O_2(b^1\Sigma_g^+, v=1)$, $O_2(a^1\Delta_g, v=0)$ and $O(^1D)$) fulfil this requirement.

The second criterion of a 'good' proxy is the value of $[O_3]$ retrieval uncertainty. In the interval of 50–98 km, ($O_2(b^1\Sigma_g^+, v=1)$) and $O(^1D)$ represent the 'good' proxy with a value of uncertainty of less than 20% below 90 km and less than 25% up to 98 km (Fig. 11). In the range of 50–85 km, $O_2(a^1\Delta_g, v=0)$ is also the available proxy, with an uncertainty value of less than 15–20%. Above 90 km, $O_2(a^1\Delta_g, v=0)$ becomes the worst proxy, with uncertainty exceeding 100%. In terms of the 'worst' proxy in the mesosphere (up to 90 km), $O_2(b^1\Sigma_g^+, v=0)$, the value of retrieval uncertainty exceeds 35% at 65–80 km (Fig. 11). However, above 90 km, the uncertainties for the $[O_3]$ retrieved from $O_2(b^1\Sigma_g^+, v=0)$ proxy becomes approximately 20–30% (Fig. 11). Therefore, $O_2(b^1\Sigma_g^+, v=1)$ is the preferable proxy at altitudes of 50–98 km. Although $O(^1D)$ satisfies both the criteria of a 'good' proxy, it cannot be recommended for $[O_3]$ retrieval due to a small intensity of red line emission ($O(^1D) \rightarrow O(^3P)$) (Section 7). It is therefore important to note that,

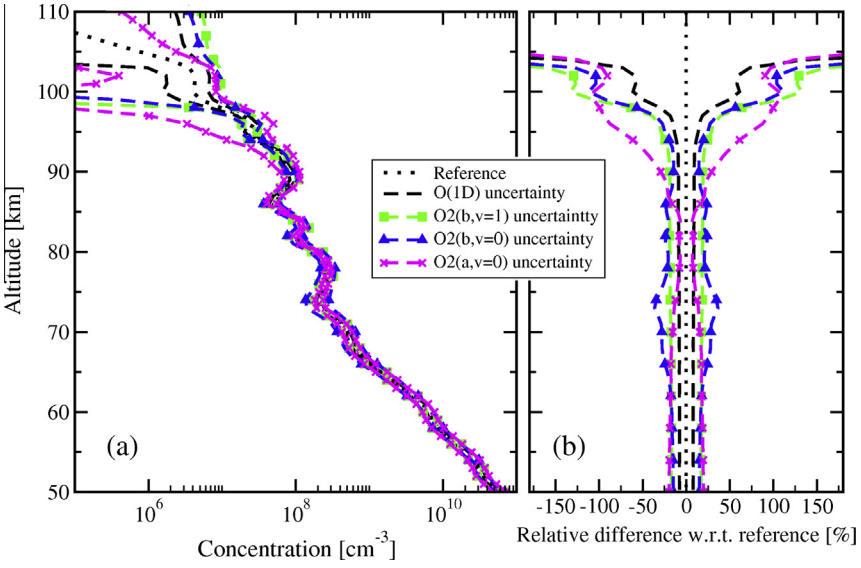

Fig. 11. Uncertainties of $[O_3]$ retrieval (the limits $\pm\sigma$) for different proxies: (a) absolute values, (b) relative values. The predetermined reference altitude profile of $[O_3]$ is presented by the dotted curve, and is taken from SABER L2, 2010, day 172, latitude 43.0, SZA = 70.5, F10.7 = 74. Type of proxy: $O(^1D)$ – dashed line; $O_2(b^1\Sigma_g^+, v=2)$ – dashed line with filled circles; $O_2(b^1\Sigma_g^+, v=1)$ – dashed line with filled squares; $O_2(b^1\Sigma_g^+, v=0)$ – dashed line with filled triangles; $O_2(a^1\Delta_g, v=0)$ – dashed line with crosses.

according to Figs. 10 and 11, at above 98 km neither of the proxies under consideration can provide ozone retrieval of sufficient accuracy.

5.4.2. [O(^{3}P)] retrieval

In Fig. 12, we show the $S(O(^3P); proxy)$ sensitivity coefficients for the inverse problem. In correspondence with (11), the $O_2(b^1\Sigma_g^+, v=2)$ is the best proxy in the 90–140 km interval. Other possible proxies of [O(^{3}P)] retrieval are $O_2(b^1\Sigma_g^+, v=0)$ in the 95–140 km altitude interval, $O_2(a^1\Delta_g, v=0)$ above 120 km and $O_2(b^1\Sigma_g^+, v=1)$ above 110 km up to 140 km.

The second criterion for the proxy choice is the value of the [O(^{3}P)] retrieval uncertainty (Fig. 13). As one can see, above 120 km the uncertainties associated with all the proxies are approximately of the same order of magnitude (25–40%). In the altitude region of 90–120 km, the minimal uncertainties for the [O(^{3}P)] retrieved from the proxies $O_2(b^1\Sigma_g^+, v=2)$ and $O_2(b^1\Sigma_g^+, v=0)$ are not more than 25% (Fig. 13). We stress here that for $k(O_2(b, v=0); O(^3P))$ we take the 'optimistic' value of uncertainty equal to 25% [13], Table A1 from Appendix A. Only above 115 km does the uncertainty of the [O(^{3}P)] retrieved from the $O_2(b^1\Sigma_g^+, v=1)$ proxy becomes about 25%. Thus, in correspondence with both criteria, $O_2(b^1\Sigma_g^+, v=2)$ is the best [O(^{3}P)] proxy in the interval of 90–140 km. For all proxies below 90 km then, our estimations of uncertainties give the values of uncertainties to be more than 100%.

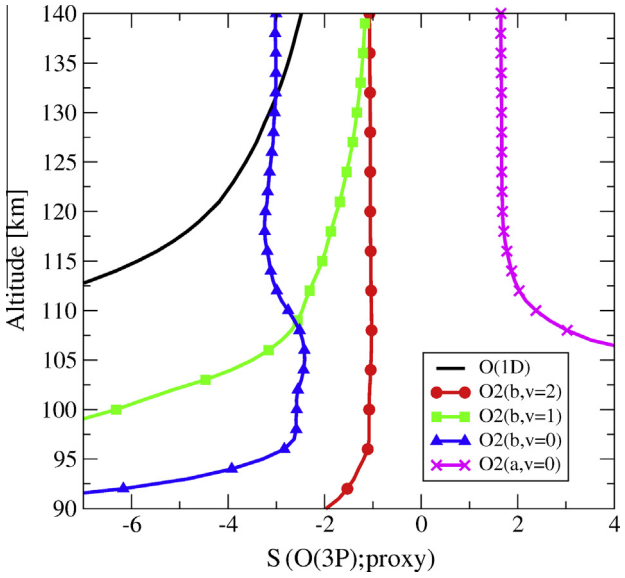

Fig. 12. Sensitivity coefficient, $S(O(^3P); proxy)$, for inverse problem of [O(^{3}P)] retrieval from proxy concentration. See the type of proxy in the caption to Fig. 8.

6. Studying the lifetimes of the excited states

The photochemical lifetime of excited state is an inverse value to the sum of the rates of radiative and collisional deactivation processes:

$$\tau(x_i) = (A_i + [O_2]\cdot k(x_i; O_2) + [O(^3P)]\cdot k(x_i; O(^3P)) + [O_3] \cdot k(x_i; O_3) + [N_2]\cdot k(x_i; N_2) + [CO_2]\cdot k(x_i; CO_2))^{-1}, \quad (13)$$

where x_i is one of the O(^{1}D), $O_2(b^1\Sigma_g^+, v=0,1,2)$, or $O_2(a^1\Delta_g, v=0)$ proxies, $k(x_i; O_2)$ is the rate coefficient of collisional deactivation from Appendix A, and $\tau(x_i)$ is the inverse value of the quenching factor $Q(x_i)$ (B1 from Appendix B). In the interval of 50–140 km, we used a reference atmospheric model retrieved from the SABER measurement for 2010, day 172, latitude 43.0, SZA = 70.5, F10.7 = 74.

As there was proposal to use $O_2(b^1\Sigma_g^+, v=1)$ as O(^{3}P) proxy in the 140–250 km altitude interval [38], we estimated the lifetimes and the contribution of collisional process with the participation of O(^{3}P) in a quenching factor. It is unfeasible to carry out the sensitivity study for the 140–250 km interval where the temperature reaches values larger than 1000 K while the vast majority of reaction rate coefficients are measured for the temperatures below 450 K. Nevertheless, estimating the lifetimes and input of O(^{3}P) in quenching factor leads one to suggest what excited species could be [O(^{3}P)] proxy up to 200 km. For the 140–200 km interval, in order to track the altitude dependence of the proxy photochemical lifetimes and the input of O(^{3}P) in the quenching factor, we used the MSISE reference atmospheric data for day and time.

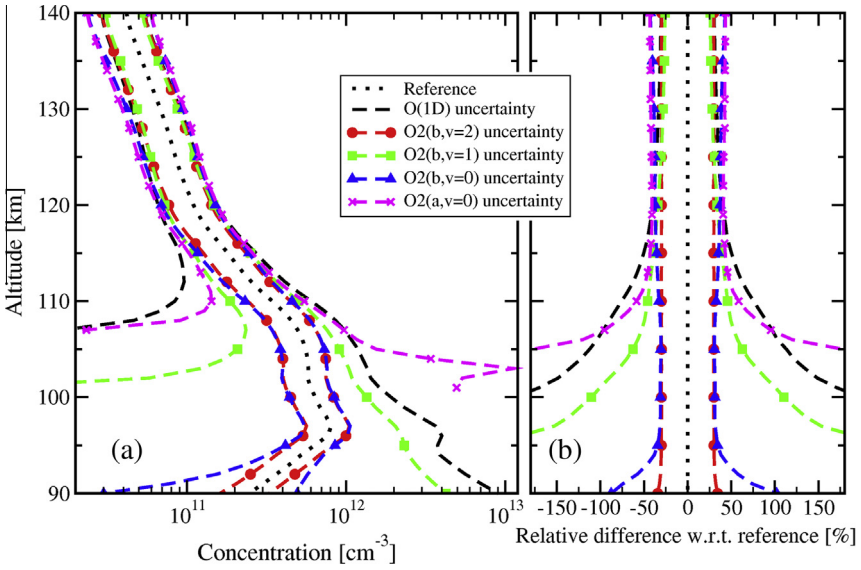

Fig. 13. Uncertainties of [O(^{3}P)] retrievals (the limits $\pm\sigma$) for different proxies: (a) absolute values, (b) relative values. The predetermined reference altitude profile of [O(^{3}P)] is presented by the dotted curve, and is taken from event SABER L2, 2010, day 172, latitude 43.0, SZA = 70.5, F10.7 = 74. See the type of proxy in the caption to Fig. 11.

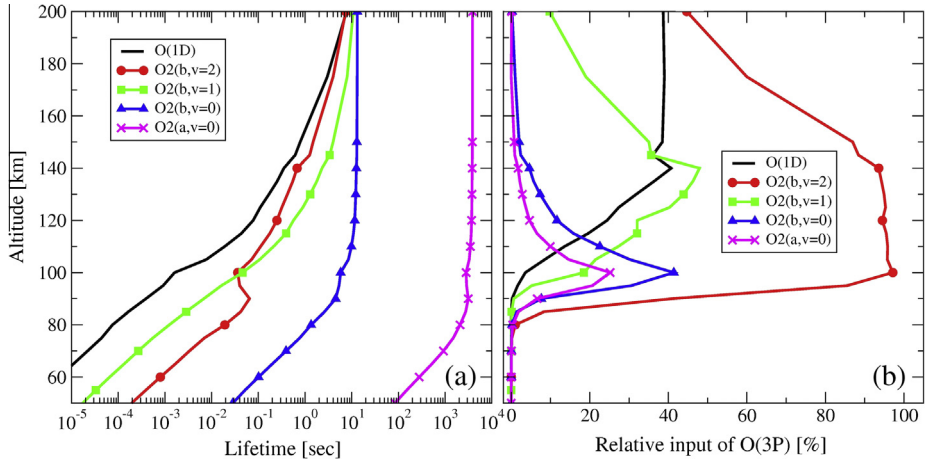

Fig. 14. (a) Typical photochemical lifetimes of proxies $O(^1D)$, $[O_2(b^1\Sigma_g^+, v=0,1,2)]$ and $O_2(a^1\Delta_g, v=0)$ in the MLT. (b) Relative input of collisional processes with the participation of $O(^3P)$ in the quenching factor for different proxies. See the type of proxy in the caption to Fig. 8.

This corresponded to the afore-mentioned SABER event and the rate coefficients when measured for the upper limit of temperature (see Appendix A).

Fig. 14a shows the typical lifetimes of all proxies in the interval of 50–200 km. The 1.27 μm O_2 IR Atmospheric band is formed from the commonly used $[O_3]$ retrieval proxy, $O_2(a^1\Delta_g, v=0)$, a transition which has more than a one hour lifetime in the MLT. On the other hand, the $O(^1D)$ and $O_2(b^1\Sigma_g^+, v=0,1,2)$ lifetime is less than 14 s in the altitude region of 50–200 km. Thus, when the $O_2(a^1\Delta_g, v=0)$ proxy becomes useless, the proposed $O(^1D)$ and $O_2(b^1\Sigma_g^+, v=0,1,2)$ proxies can then be used for tracking fast variations of the $O(^3P)$ and O_3 atmospheric concentrations generated by wave processes, electron precipitations, solar flux changes and so on.

In correspondence with the afore-mentioned suggestions for estimating the possibility of $[O(^3P)]$ retrieval based on the role of $O(^3P)$ as a quencher of $O_2(b^1\Sigma_g^+, v=1)$ in the 140–250 km interval [38], we calculated the quenching factor q for all five proxies up to 200 km. Fig. 14b shows the role of $O(^3P)$ as a quencher of electronic-vibrational excitation of $O_2(b^1\Sigma_g^+, v=0,1,2)$, $O_2(a^1\Delta_g, v=0)$ and $O(^1D)$. Based on these qualitative estimations, one can see that $O(^3P)$ dominates in the $O_2(b^1\Sigma_g^+, v=2)$ quenching in the 85–200 km altitude interval. From this perspective, $O(^1D)$ and $O_2(b^1\Sigma_g^+, v=1)$ can also be considered for $[O(^3P)]$ retrieval in the interval of 115–200 km and 100–175 km, respectively. The quenching factor for the remaining two proxies, $O_2(b^1\Sigma_g^+, v=0)$ and $O_2(a^1\Delta_g, v=0)$, depends on $[O(^3P)]$ but only in the 90–120 km interval. Therefore, above 140 km and up to 200 km, the qualitative estimations of Fig. 14b show that $O_2(b^1\Sigma_g^+, v=2)$ and $O(^1D)$ are more suitable proxies of $O(^3P)$ than $O_2(b^1\Sigma_g^+, v=1)$ because the quenching factor q of the latter decreases sharply above 140 km and reaches 10% at 200 km.

7. Volume emission rates (VER)

In this section, we provide the estimates of proxy radiances; namely, volume emission rates (VER) for radiative transitions originated from excited levels $O_2(b^1\Sigma_g^+, v=0,1,2)$, $O_2(a^1\Delta_g, v=0)$, and $O(^1D)$. The transitions are represented in Fig. 1 by vertical lines with the arrows pointed down. The wavelengths of band centres and the Einstein coefficients of radiative transitions are provided in Table 7.1 (see also Table B2).

In Table 7.1 the Atmospheric bands centres have been calculated using the data from the GEISA database [53]. The Einstein coefficients in [30] have also been estimated using the approach of [54] and the values of the Franck–Condon factors of [50].

The volume emission rate of the corresponding Atmospheric bands is defined as follows:

$$\mathrm{VER} = [O_2(b^1\Sigma_g^+, v')] \cdot A(b^1\Sigma_g^+, v' \to X, v''), \tag{14}$$

Table 7.1
Wavenumbers of Atmospheric band centres and the Einstein coefficient of corresponding transitions.

Electronic-vibrational band	Vibrational levels		Center of band		$A(*, v' \to X, v'')$ Einstein coefficient (s^{-1})	Reference
	v'	v''	ν (cm^{-1})	λ (nm)		
$O_2(a^1\Delta_g, v' \to X^3\Sigma_g^-, v'')$	0	0	7882.8	1268.6	2.26E−04	[49]
	0	1	6326.4	1580.4	2.81E−06	[50]
$O_2(b^1\Sigma_g^+, v' \to X^3\Sigma_g^-, v'')$	0	0	13121.1	762.1	8.34E−02	[51]
	0	1	11564.7	864.7	4.67E−03	[52]
	0	2	10031.9	996.8	8.8E−05	[30]
	1	0	14525.8	688.4	7.2E−03	[51]
	1	1	12969.4	771.0	7.2E−02	[52]
	1	2	11436.6	874.4	6.9E−03	[30]
	2	0	15902.6	628.8	3.24E−04	[52]
	2	1	14346.2	697.0	1.4E−02	[30]
	2	2	12813.4	780.4	4.8E−02	[30]

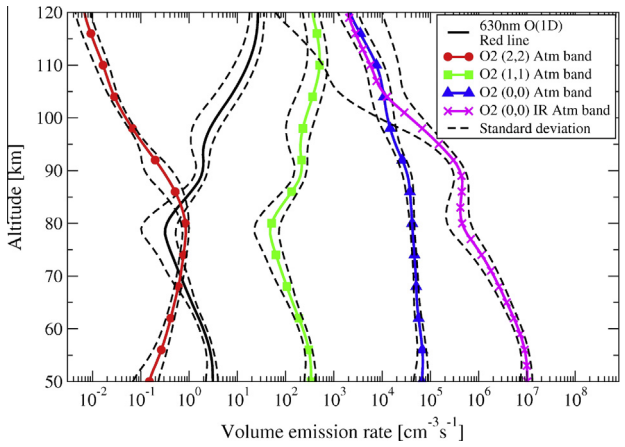

Fig. 15. Volume emission rates (VER) for red line $O(^1D) \rightarrow O(^3P)$ transition, and four Atmospheric bands $O_2(b^1\Sigma_g^+, v=2 \rightarrow X^3\Sigma_g^-, v=2)$, $O_2(b^1\Sigma_g^+, v=1 \rightarrow X^3\Sigma_g^-, v=1)$, $O_2(b^1\Sigma_g^+, v=0 \rightarrow X^3\Sigma_g^-, v=0)$, $O_2(a^1\Delta_g, v=0 \rightarrow X^3\Sigma_g^-, v=0)$. Solid and dashed curves are the mean VER and their standard deviations for 150 SABER events during 22nd September 2010 (Latitudes from −43.8° to 75.0°; SZA from 46.0° to 82.0°) correspondingly. See the type of proxy in the caption to Fig. 8. (For interpretation of the references to colour in this figure legend, the reader is referred to the web version of this article.)

where $A(b^1\Sigma_g^+, v' \rightarrow X, v'')$ is the Einstein coefficient (in s^{-1}) of corresponding transition (Table 7.1), and the units of VER are [$cm^{-3}\ s^{-1}$]. A similar expression for the volume emission rate is valid for IR Atmospheric band $O_2(a^1\Delta_g, v'=0 \rightarrow X^3\Sigma_g^-, v''=0)$ and Red line $O(^1D \rightarrow {}^3P)$.

Fig. 15 shows the VERs of the most intensive emissions listed in Table 7.1, the ones that we would suggest using. In terms of the mean values and the dispersions of the intensities of the emissions (14), we have used calculated altitude profiles of the proxy concentrations for 150 events of SABER taking place on 22nd September 2010 (Latitudes from −43.8° to 75.0°; SZA from 46.0° to 82.0°) as presented in Fig. 2 for $[O_2(b^1\Sigma_g^+, v=0,1,2)]$.

Table 7.1 and the estimations made with the help of Fig. 15 thus allow qualitative characterisation of all the proxies in terms of signal intensity; the latter can help in choosing the detection system for the experiment. It is worth noting that the minimum of $O_2(b^1\Sigma_g^+, v=2 \rightarrow X^3\Sigma_g^-, v=2)$ emission is comparable with Red line emission up to 90 km. It is essential that the most intensive transitions from $O_2(b^1\Sigma_g^+, v=1$ and $v=2)$ Atmospheric bands (1,1), (1,2), (2,1) and (2,2) are optically thin above 50 km.

8. Discussion

The analysis of $O_2(a^1\Delta_g, v=0–5)$, $O_2(b^1\Sigma_g^+, v=0,1,2)$ and $O(^1D)$ altitude distributions allows one to consider these levels as the $[O_3]$ and $[O(^3P)]$ proxies in the MLT region (their populations are governed by concentrations of these atmospheric species). As a result, we have selected five proxies: $O_2(a^1\Delta_g, v=0)$, $O_2(b^1\Sigma_g^+, v=0,1,2)$, and $O(^1D)$.

8.1. Influence of the internal parameters of model YM2011 on the altitude profiles of $O(^3P)$ and O_3 concentrations retrieval using the suggested proxies

The main source of uncertainty in the complex photochemical system modelling is associated with the internal parameters of the model; namely, the rate coefficient errors and quantum yields of the products of the aeronomical reactions. The relative errors of these parameters range from four percent and up to several hundred percent (see experimentally determined values of ξ_i in Appendix A). We have also considered the temperature dependence of the rate coefficients (Appendix A). In order to estimate the individual influence of the model parameters (atmospheric temperature, rate coefficients and quantum yields of the products of aeronomical reactions) on the $[O_3]$ or $[O(^3P)]$ retrievals, we changed the corresponding parameter by the experimental value of its uncertainty, ξ_i, and solved the inverse problem for each proxy under consideration. Table 8.1 demonstrates the corresponding impact on $[O_3]$ or $[O(^3P)]$ retrieval. We have tested the influence of the model parameters on the altitude profiles of $O(^3P)$ and O_3 concentrations retrieved using five proxies: $O_2(b^1\Sigma_g^+, v=0,1,2)$, $O_2(a^1\Delta_g, v=0)$, and $O(^1D)$. The strength of influence present in Table 8.1 is as follows. If the variation of the corresponding parameter by its experimental uncertainty, ξ_i, leads to more than 30% change in the retrieved $[O(^3P)]$ or $[O_3]$, then it is marked by "+++". The "++" and "+" symbols stand for 3–30% and 1–3% change, respectively, while "−" means no influence and "n/d" means the absence of data (see Appendix A).

Based on the impact analysis, the results of which are presented in Table 8.1, we conclude that:

(a) In consideration of the complexity of kinetics of the excited components, choosing $O(^1D)$ as a proxy for $[O_3]$ and $[O(^3P)]$ retrieval requires taking into account five aeronomical reactions. For other proxies, the number of aeronomical reactions is as follows: $O_2(b^1\Sigma_g^+, v=2)$ – five; $O_2(b^1\Sigma_g^+, v=1)$–13; $O_2(b^1\Sigma_g^+, v=0)$–18; $O_2(a^1\Delta_g, v=0)$–25. Increasing the number of reactions that must be considered when using a proxy from $O(^1D)$, $O_2(b^1\Sigma_g^+, v=2)$, $O_2(b^1\Sigma_g^+, v=1)$, $O_2(b^1\Sigma_g^+, v=0)$ to $O_2(a^1\Delta_g, v=0)$ depends on the requirement that, when calculating the population of each of the underlying electronic-vibrationally excited states, one takes account of the mechanisms of the population of the upper levels (Fig. 1).

(b) The choice of the $O_2(b^1\Sigma_g^+, v=0)$ and $O_2(a^1\Delta_g, v=0)$, the transitions from which form the most intensive bands, is associated with the problem of there being poorly known rate coefficients for some important processes: e.g., $O_2(b^1\Sigma_g^+, v=0) + O(^3P) \rightarrow$ *products*, $O_2(a^1\Delta_g, v \geqslant 1) + O_3 \rightarrow$ *products* and $O_2(a^1\Delta_g, v=0) + O(^3P) \rightarrow$ *products*, etc.

(c) The temperature variation dependencies of $[O_2(b^1\Sigma_g^+, v=1)]$ and $[O(^1D)]$ are much more significant than for the other proxies because the rates of key reactions for these proxies (usually collisional processes with N_2 and O_2) strongly depend on gas temperatures.

One can use the results of this analysis (Table 8.1) for the optimal choice of the $O(^3P)$ or O_3 retrieval approach taking into account the kinetic data available.

8.2. Optimal methods of $[O(^3P)]$ and $[O_3]$ retrieval

Using the uncertainty analysis presented in Section 5.4, we may conclude that for the $[O(^3P)]$ retrieval, $O_2(b^1\Sigma_g^+, v=0–2)$ are preferable proxies in view of the uncertainty of the $[O(^3P)]$ altitude profile retrieval, which is about 25–30%. This is true for $O_2(b^1\Sigma_g^+, v=2)$ in the altitude range of 90–140 km, for $O_2(b^1\Sigma_g^+, v=1)$ only in the range of 110–140 km and for $O_2(b^1\Sigma_g^+, v=0)$ above 95 km (Fig. 13). However, the intensities are relatively low of the (2,2),

(2,1) and (2,0) Atmospheric bands formed by transitions from level $O_2(b^1\Sigma_g^+, v=2)$ (Fig. 15). Other possible proxies of [$O(^3P)$] retrieval with the same uncertainties are $O_2(b^1\Sigma_g^+, v=0)$ in the 95–140 km altitude interval and $O_2(b^1\Sigma_g^+, v=1)$ above 110 km and up to 140 km. It is worth noting that for all proxies retrieval of the [$O(^3P)$], the altitude profile does not depend on [O_3] altitude distribution above 105 km because the corresponding sensitivity coefficient is close to zero (Fig. 8).

The least suitable proxy is $O_2(a^1\Delta_g, v=0)$ for which the minimal uncertainty is more than 40% only above 120 km (Fig. 13). Hedin et al. [55] have suggested using the measured emissions $O(^1D \rightarrow {}^3P)$ and $O_2(b^1\Sigma_g^+, v=1 \rightarrow X^3\Sigma_g^-, v=1)$ as a comprehensive tool for measuring temperature and atomic oxygen in the thermosphere. As one can see from Fig. 13, this method could be used above 125 km because, at the lower altitudes, the uncertainties of retrieved [$O(^3P)$] sharply increase and reach 50% near 115 km.

Concerning the [O_3] retrieval in the range of 50–100 km, the emissions at 1.27 μm formed by transition from $O_2(a^1\Delta_g, v=0)$ and at 762 nm formed by transition from $O_2(b^1\Sigma_g^+, v=0)$ are the most intensive ones amongst all the emissions under consideration (Fig. 15). However, these two proxies cannot be admitted as the best ones for ozone retrieval because of the large values of the corresponding uncertainties. For the first of them, the uncertainty reaches 100% above 90 km, while for the second it exceeds 35% in the 65–75 km altitude range. This makes $O_2(b^1\Sigma_g^+, v=1)$ and $O(^1D)$ the optimal proxies for O_3 in the range 50–98 km, with uncertainties of about 15–20%, shown by the sensitivity study in Section 5 (Fig. 11). Nevertheless, in the range of 84–96 km $O_2(b^1\Sigma_g^+, v=0)$ and in the interval 50–85 km $O_2(a^1\Delta_g, v=0)$ can be used as O_3 proxy (Fig. 11). Below 90 km, the retrieval of [O_3] vertical profiles does not depend on [$O(^3P)$] altitude distribution because the corresponding sensitivity coefficient is close to zero (Fig. 9).

Table 8.1
Influence of the model parameters on the altitude profiles of [$O(^3P)$] and [O_3].

Parameters of the model: rate coefficients of mentioned reactions, quantum yield (F), gas temperature (T_n)	ξ	Proxies for retrieval of [$O(^3P)$] or [O_3]									
		$O(^1D)$		$O_2(b^1\Sigma_g^+, v=2)$		$O_2(b^1\Sigma_g^+, v=1)$		$O_2(b^1\Sigma_g^+, v=0)$		$O_2(a^1\Delta_g, v=0)$	
		[$O(^3P)$]	[O_3]	[$O(^3P)$]	[O_3]	[$O(^3P)$]	[O_3]	[$O(^3P)$]	[O_3]	[$O(^3P)$]	[O_3]
T_n		++	++	+	–	++	++	+	+	+	+
$O(^1D) + O(^3P) \rightarrow$	±0.27	+++	+	–	–	++	+	++	+	++	+
$O(^1D) + O_2 \rightarrow$	±0.08	++	++	–	–	++	++	+++	++	++	+
$F(O(^1D) \rightarrow O_2(b^1\Sigma_g^+, v=1); O_2)$	±0.125	–	–	–	–	+++	+++	++	+	++	++
$O(^1D) + O_3 \rightarrow$	±0.15	+	+	–	–	+	+	+	+	+	+
$O(^1D) + N_2 \rightarrow$	±0.10	+++	+++	–	–	++	++	+++	++	++	+
$O(^1D) + CO_2 \rightarrow$	±0.15	+	+	–	–	+	+	+	+	+	+
$O_2(b^1\Sigma_g^+, v=2) + O(^3P) \rightarrow$	±0.60	–	–	+++	–	+	+	+	+	+	+
$O_2(b^1\Sigma_g^+, v=2) + O_2 \rightarrow$	±0.07	–	–	+	–	+	+	+	+	+	+
$O_2(b^1\Sigma_g^+, v=2) + O_3 \rightarrow$	±0.40	–	–	+	–	+	+	+	+	++	+
$O_2(b^1\Sigma_g^+, v=2) + N_2 \rightarrow$	±0.40	–	–	+	–	+	+	+	+	+	+
$O_2(b^1\Sigma_g^+, v=2) + CO_2 \rightarrow$	±0.30	–	–	+	–	+	+	+	+	+	+
$O_2(b^1\Sigma_g^+, v=1) + O(^3P) \rightarrow$	0.18/−0.29	–	–	–	–	++	+	++	+	+	+
$O_2(b^1\Sigma_g^+, v=1) + O_2 \rightarrow$	±0.40	–	–	–	–	++	++	+	+	+	+
$O_2(b^1\Sigma_g^+, v=1) + O_3 \rightarrow$	n/d	–	–	–	–	+	+	+	+	+	+
$O_2(b^1\Sigma_g^+, v=1) + N_2 \rightarrow$	n/d	–	–	–	–	+	+	+	+	+	+
$O_2(b^1\Sigma_g^+, v=1) + CO_2 \rightarrow$	±0.60	–	–	–	–	+	+	+	+	+	+
$O_2(b^1\Sigma_g^+, v=0) + O(^3P) \rightarrow$	4.0/−0.8	–	–	–	–	–	–	+++	+	+++	+
$O_2(b^1\Sigma_g^+, v=0) + O_2 \rightarrow$	±0.50	–	–	–	–	–	–	+	+	+	+
$O_2(b^1\Sigma_g^+, v=0) + O_3 \rightarrow$	±0.15	–	–	–	–	–	–	+	+	+	+
$O_2(b^1\Sigma_g^+, v=0) + N_2 \rightarrow$	±0.10	–	–	–	–	–	–	+	+++	+	+
$O_2(b^1\Sigma_g^+, v=0) + CO_2 \rightarrow$	±0.20	–	–	–	–	–	–	+	+	+	+
$O_2(a^1\Delta_g, v \geqslant 2) + O(^3P) \rightarrow$	n/d	–	–	–	–	–	–	–	–	+	+
$O_2(a^1\Delta_g, v \geqslant 2) + O_2 \rightarrow$	±0.11	–	–	–	–	–	–	–	–	+	+
$O_2(a^1\Delta_g, v \geqslant 2) + O_3 \rightarrow$	±0.43	–	–	–	–	–	–	–	–	+	++
$O_2(a^1\Delta_g, v \geqslant 2) + N_2 \rightarrow$	n/d	–	–	–	–	–	–	–	–	+	+
$O_2(a^1\Delta_g, v \geqslant 2) + CO_2 \rightarrow$	n/d	–	–	–	–	–	–	–	–	+	+
$O_2(a^1\Delta_g, v=1) + O(^3P) \rightarrow$	n/d	–	–	–	–	–	–	–	–	+	+
$O_2(a^1\Delta_g, v=1) + O_2 \rightarrow$	±0.20	–	–	–	–	–	–	–	–	+	+
$O_2(a^1\Delta_g, v=1) + O_3 \rightarrow$	±0.43	–	–	–	–	–	–	–	–	+	++
$O_2(a^1\Delta_g, v=1) + N_2 \rightarrow$	n/d	–	–	–	–	–	–	–	–	+	+
$O_2(a^1\Delta_g, v=1) + CO_2 \rightarrow$	±0.08	–	–	–	–	–	–	–	–	+	+
$O_2(a^1\Delta_g, v=0) + O(^3P) \rightarrow$	2.0/−0.7	–	–	–	–	–	–	–	–	++	++
$O_2(a^1\Delta_g, v=0) + O_2 \rightarrow$	±0.20	–	–	–	–	–	–	–	–	+	+++
$O_2(a^1\Delta_g, v=0) + O_3 \rightarrow$	±0.25	–	–	–	–	–	–	–	–	+	+
$O_2(a^1\Delta_g, v=0) + N_2 \rightarrow$	n/d	–	–	–	–	–	–	–	–	+	+
$O_2(a^1\Delta_g, v=0) + CO_2 \rightarrow$	n/d	–	–	–	–	–	–	–	–	+	+

There is a fundamental problem complicating the retrieval of vertical profiles of $[O_3]$ and $[O(^3P)]$ in the region of 90–105 km. In this range, the $[O_3]$ altitude profile retrieval requires knowing the $[O(^3P)]$ altitude profile and vice versa (see Section 5, Figs. 3–7). This problem can be solved by a simultaneous retrieval of the $[O_3]$ and $[O(^3P)]$ altitude distributions that requires two proxies. There are two variants: (a) if one chooses $O_2(b^1\Sigma_g^+, v=2)$ as a proxy for $[O(^3P)]$ retrieval, then either $O_2(b^1\Sigma_g^+, v=1)$ or $O_2(b^1\Sigma_g^+, v=0)$ can be used for $[O_3]$ retrieval; (b) if one chooses $O_2(b^1\Sigma_g^+, v=0)$ as the proxy for $[O(^3P)]$ retrieval, then either $O_2(b^1\Sigma_g^+, v=1)$ or $O(^1D)$ can be used for the $[O_3]$ retrieval.

8.3. Analytical formulae for $[O_3]$ and $[O(^3P)]$ retrieval

The sensitivity study enables one to obtain the approximate analytical formulae for $[O_3]$ and $[O(^3P)]$ retrieval using proxies $O_2(b^1\Sigma_g^+, v=0)$, $O_2(b^1\Sigma_g^+, v=1)$, $O_2(b^1\Sigma_g^+, v=2)$ and $O(^1D)$.

Here we discuss only $O_2(b^1\Sigma_g^+, v=1)$, since [55] have suggested carrying out the rocket experiment to measure $[O(^3P)]$ in the lower thermosphere using the observations of emission intensity from this excited state at 771 nm, Atmospheric band (1,1). The emission from $O_2(b^1\Sigma_g^+, v=1)$ can be measured in three spectral channels: 688, 771 and 874 nm (Table 7.1). The total volume emission rate of these bands is about 10^2–10^3 photon cm^{-3} s^{-1}. We have shown that $O_2(b^1\Sigma_g^+, v=1)$ could be used not only for $[O(^3P)]$ retrieval from 90 to 140 km, but also for $[O_3]$ retrieval in the 50–98 km altitude range (Sections 5.4 and 8.2).

The sensitivity study shows that the following processes can be excluded from the kinetic equations built for the 50–140 km region. First, all energy transfer processes from $O_2(b^1\Sigma_g^+, v=2)$ to $O_2(b^1\Sigma_g^+, v=1)$, mainly at collisions with the molecules of atmospheric gases, for which the sensitivity coefficient of $[O_2(b^1\Sigma_g^+, v=1)]$ to $[O_2(b^1\Sigma_g^+, v=2)]$, $S(O_2(b^1\Sigma_g^+, v=1); O_2(b^1\Sigma_g^+, v=2))$, is less than 0.01%. Second, the $O(^1D) + O_3 \rightarrow O_2 + 2O(^3P)$ reaction can also be excluded because of the small value of the sensitivity coefficient, $S(O(^1D); k(O(^1D); O_3))$ (see Fig. 3–5 and Table C1 in Appendix C).

In regard to these simplifications, we obtain the stationary balance equation for $[O_2(b^1\Sigma_g^+, v=1)]$ with less than 0.1% uncertainty compared to exact Eq. (9):

$$\left[O_2\left(b^1\Sigma_g^+,\ v=1\right)\right] = \frac{[O_2]\cdot\left(\frac{k(O(^1D);O_2)\cdot\psi\cdot([O_2]\cdot(J_{SRC}+J_{Ly\,\alpha}\cdot F(Ly\ \alpha))+[O_3]\cdot J_{HB}\cdot F(HB\rightarrow O(^1D))}{Q(O(^1D))}+g_\beta\right)}{Q\left(O_2\left(b^1\Sigma_g^+,\ v=1\right)\right)} \quad (15)$$

where $\psi = F(O(^1D) \rightarrow O_2(b, v=1); O_2)$ – quantum yield of $O_2(b^1\Sigma_g^+, v=1)$ in the reaction $O(^1D) + O_2 \rightarrow O(^3P) + O_2(b^1\Sigma_g^+, v)$.

From (15) we have derived analytical formula for $[O_3]$ retrieval from proxy $O_2(b^1\Sigma_g^+, v=1)$:

$$[O_3] = \frac{\left(\left[O_2\left(b^1\Sigma_g^+, v=1\right)\right]\cdot Q\left(O_2\left(b^1\Sigma_g^+, v=1\right)\right) - [O_2]\cdot g_\beta\right)\cdot Q(O(^1D))}{J_{HB}\cdot F(HB\rightarrow O(^1D))\cdot[O_2]\cdot k(O(^1D);O_2)\cdot\psi} - \frac{[O_2]\cdot(J_{SRC}+J_{Ly\,\alpha}\cdot F(Ly\,\alpha))}{J_H\cdot F(HB\rightarrow O(^1D))} \quad (16)$$

Formula (16) enables one to retrieve $[O_3]$ in the interval of 50–98 km. Below 90 km, the $O(^3P)$ concentration does not affect the $[O_3]$ retrieval because the sensitivity coefficient of $O_2(b^1\Sigma_g^+, v=1)$ to $O(^3P)$ is less than 0.05 (see Fig. 5).

From (15), we derive analytical formula for $[O(^3P)]$ retrieval from proxy $O_2(b^1\Sigma_g^+, v=1)$:

$$[O(^3P)] = \frac{B-A}{2} + \sqrt{\frac{(A+B)^2}{4}+C} \quad (17)$$

where

$$A = \frac{[O_2]\cdot(k(O(^1D);O_2) + [N_2]\cdot k(O(^1D);N_2) + [CO_2]\cdot(k(O(^1D);CO_2)}{k(O(^1D);O(^3P))}$$

$$B = \frac{[O_2]\cdot g_\beta - \left[O_2\left(b^1\Sigma_g^+,\ v=1\right)\right]\cdot\left(A_{O_2(b,\ v=1)} + [O_2]\cdot k(O_2(b,\ v=1);O_2) + [CO_2]\cdot k(O_2(b,\ v=1);CO_2)\right)}{\left[O_2\left(b^1\Sigma_g^+,\ v=1\right)\right]\cdot k(O_2(b,\ v=1);O(^3P))}$$

$$C = \frac{[O_2]\cdot(k(O(^1D);O_2)\cdot\psi\cdot([O_2]\cdot(J_{SRC}+J_{Ly\,\alpha}\cdot F(Ly\ \alpha)) + [O_3]\cdot J_{HB}\cdot F(HB\rightarrow O(^1D))}{\left[O_2\left(b^1\Sigma_g^+,\ v=1\right)\right]\cdot k(O_2(b,\ v=1);O(^3P))\cdot k(O(^1D);O(^3P))}$$

The information source of the concentration of atomic oxygen in (17) is the concentration of the proxy $O_2(b^1\Sigma_g^+, v=1)$, included in the terms B and C.

Formula (17) enables one to retrieve $[O(^3P)]$ in the interval of 100–140 km with an error smaller than 0.1%, compared to exact Eq. (9). In this altitude interval, the influence of O_3 concentration is negligibly small. From 100 to 90 km, the error increases and reaches as much as 5% at 90 km due to the growing influence of ozone on a population of $O_2(b^1\Sigma_g^+, v=1)$. Below 90 km, formula (17) cannot be used.

9. Conclusions

1. In the framework of model YM2011, we have described the kinetics of 10 excited levels: $O(^1D)$, three levels $O_2(b^1\Sigma_g^+, v \leqslant 2)$, six levels $O_2(a^1\Delta_g, v \leqslant 5)$. The methodology developed in YM2011 allows us to solve the system of 10 kinetic equations for populations of electronically–vibrationally excited levels of oxygen molecule $O_2(a^1\Delta_g, v=0$–$5)$, $O_2(b^1\Sigma_g^+, v=0,1,2)$ and excited oxygen atom $O(^1D)$. The system of kinetic equations for modelling the electronic-vibrational kinetics of excited oxygen molecules in the MLT region is presented in explicit form in Appendix B.

2. For the first time we present an overview of the reaction rates for the collisions between $O_2(b^1\Sigma_g^+, v \leqslant 2)$, $O_2(a^1\Delta_g, v \leqslant 5)$, $O(^1D)$ and molecules of five main atmospheric components ($O(^3P)$, O_2, N_2, O_3, and CO_2) as well as quantum yields of the products of these processes with the measured errors of these factors taking into account the experimental temperature dependence and temperature range of measurements (Appendix A).
3. Basing on the forward problem solution, we have picked up five excited components; namely, $O_2(b^1\Sigma_g^+, v = 0,1,2)$, $O_2(a^1\Delta_g, v = 0)$ and $O(^1D)$. To compare the characteristics of the assumed proxies, we have performed a sensitivity analysis of the forward calculations to $[O_3]$ and $[O(^3P)]$, and of the inverse problem of $[O_3]$ and $[O(^3P)]$ altitude profile retrieval to all parameters of the YM2011 model (more than 60). After that, we carried out the comparative analysis of sensitivity of all the proxies to $[O_3]$ and $[O(^3P)]$ and vice versa for the inverse problem of $[O_3]$ and $[O(^3P)]$ retrieval to proxy concentration. We have presented analytical expressions of sensitivity coefficients for forward and inverse problems in framework YM2011 model in Appendix C.
4. The sensitivity study of forward and reverse problems enables one to obtain the approximate analytical formulae for $[O_3]$ and $[O(^3P)]$ retrieval using proxies $O_2(b^1\Sigma_g^+, v = 1)$ (Section 8.3).
5. The $[O_3]$ retrieval can be split into two altitude ranges: 50–90 km and 90–105 km. Below 90 km, the sensitivity study (Section 5) shows that proxies $O_2(b^1\Sigma_g^+, v = 1)$, $O_2(a^1\Delta_g, v = 0)$ and $O(^1D)$ are suitable with the uncertainties of retrieved values of less than 20%. $O_2(b^1\Sigma_g^+, v = 0)$ is the 'worst' proxy in the mesosphere because, at 65–75 km, the value of uncertainty of retrieved $[O_3]$ exceeds 35%. For all these proxies, the $O(^3P)$ concentration is not important because the sensitivity coefficients, $S(proxy; O(^3P))$ are less than 0.01. As for $O_2(b^1\Sigma_g^+, v = 2)$, it is not sensitive to ozone with the corresponding sensitivity coefficient $S(O_3; O_2(b^1\Sigma_g^+, v = 2))$ smaller than 0.001. Above 90 km, $O_2(a^1\Delta_g, v = 0)$ becomes unacceptable as the $[O_3]$ proxy with uncertainty exceeding 100%. In the altitude region of 90–98 km, the minimal uncertainties for the $[O_3]$ retrieved from $O_2(b^1\Sigma_g^+, v = 1)$ and $O_2(b^1\Sigma_g^+, v = 0)$ proxies are approximately20–30%. Therefore, $O_2(b^1\Sigma_g^+, v = 1)$ is preferable for the whole altitude range 50–98 km. It should also be emphasised that, above 90 km for $[O_3]$ retrieval, one has to know the $[O(^3P)]$ altitude profile (Section 5.1).
6. For $[O(^3P)]$ retrieval, $O_2(b^1\Sigma_g^+, v = 2)$ is the best proxy in the 90–140 km interval, with uncertainty of about 25%. Above 90 km, $[O_2(b^1\Sigma_g^+, v = 2)]$ altitude profiles do not depend on $[O_3]$, while the sensitivity coefficient $S(O_2(b^1\Sigma_g^+, v = 2); O_3)$ is smaller than 0.01. Due to the low intensity of emissions formed by transitions from $O_2(b^1\Sigma_g^+, v = 2)$, we have also considered other proxies. The possible proxies for $[O(^3P)]$ retrieval are $O_2(b^1\Sigma_g^+, v = 0)$ in the 95–130 km altitude interval and $O_2(b^1\Sigma_g^+, v = 1)$ above 110 km and up to 140 km with the same uncertainties. For $[O(^3P)]$ retrieval from $[O_2(b^1\Sigma_g^+, v = 0)]$, one has to know the $[O_3]$ altitude profile. Having knowledge of $O_2(a^1\Delta_g, v = 0)$ and $O(^1D)$ enables one to estimate $[O(^3P)]$ only above 120 km with uncertainties of more than 40%.
7. In the altitude range of 90–105 km, the simultaneous retrieval of the $[O_3]$ and $[O(^3P)]$ altitude profiles requires two proxies. There are two variants here: (a) choosing $O_2(b^1\Sigma_g^+, v = 2)$ as a proxy for $[O(^3P)]$ retrieval with either $O_2(b^1\Sigma_g^+, v = 1)$ or $O_2(b^1\Sigma_g^+, v = 0)$ used as a proxy for $[O_3]$ retrieval; (b) choosing $O_2(b^1\Sigma_g^+, v = 0)$ as a proxy for $[O(^3P)]$ retrieval, with either $O_2(b^1\Sigma_g^+, v = 1)$ or $O(^1D)$ used as a proxy for $[O_3]$ retrieval.
8. A sensitivity study and uncertainty analysis have been presented in this work, as well as the calculated volume emission rates (VER) for radiative transitions originating from excited levels $O_2(b^1\Sigma_g^+, v = 0,1,2)$. Thus, $O_2(a^1\Delta_g, v = 0)$ and $O(^1D)$ and estimations of altitude dependence of the proxy photochemical lifetimes have enabled us to choose a strategy for planning the space borne experiments on the $[O(^3P)]$ and $[O_3]$ retrieval.

To summarise, we have developed the new methods of $[O(^3P)]$ and $[O_3]$ retrieval in the framework of the YM2011 model. These utilise electronic-vibrational transitions from the oxygen molecule second singlet level ($O_2(b^1\Sigma_g^+, v = 0,1,2)$. For $[O_3]$ retrieval, we recommend $O_2(a^1\Delta_g, v = 0)$ below 90 km and in the range 50–98 km $O_2(b^1\Sigma_g^+, v = 1)$ as proxies. The optimal proxies for $[O(^3P)]$ retrieval in the range of 90–140 km $O_2(b^1\Sigma_g^+, v = 2)$ is in the range of 95–140 km $O_2(b^1\Sigma_g^+, v = 0)$ and in the range 110–140 km $O_2(b^1\Sigma_g^+, v = 1)$. We have both proposed and justified the indirect methods of the $[O(^3P)]$ retrieval independently from $[O_3]$ retrieval and vice versa. Thus, where $[O(^3P)]$ and $[O_3]$ are coupled in the range of 90–105 km, we recommend a "method of two proxies" for simultaneous retrievals.

Acknowledgments

The authors are very grateful to Prof. T.G. Slanger (SRI International, Menlo Park, California) for many fruitful discussions of this work. The authors also remember with gratitude Prof. G. Witt (Stockholm University) who passed away in 2014 and whose persistent interest to these studies inspired them for many years. The funding of V.Y. and R.M. was partly provided by RFBR, grant N 09-05-00 694-a.

Appendix A

A.1. Current status of chemical kinetics data for modelling of electronic-vibrational kinetics of excited oxygen molecules in the MLT region

We present the compilation of kinetic data for 10 excited oxygen species, namely, for the energy transfer processes, which take place at collisions of electronic-vibrationally excited molecules $O_2(b^1\Sigma_g^+, v = 0,1,2)$ and $O_2(a^1\Delta_g, v = 0–5)$ and oxygen atom $O(^1D)$ with the main atmospheric components $O(^3P)$, O_2, N_2, O_3 and CO_2. We used measurements of the reaction rate coefficients mainly for last 15 years. If the quantum yields of excited products have been measured, their values are also presented in Table A1. For the whole model YM2011 the complete sets of the rate coefficients and quantum yields of products of reactions for 35 levels $O_2(X^3\Sigma_g^-, v = 1–35)$ were presented in [9] and all photoprocesses were introduced in [1].

Below we describe the notations and different details of used kinetic data:

a. Short notations of levels: $O_2(b^1\Sigma_g^+, v) = O_2(b, v)$, $O_2(a^1\Delta_g, v) = O_2(a, v)$ and $O_2(X^3\Sigma_g^-, v) = O_2(X, v)$.
b. $k(A^*; B)$ is the rate constant for bimolecular reaction $A^* + B \rightarrow C^{**} + D$, following the traditional form that was used by Sir D.R. Bates in the 1980s.

Table A1
Rate coefficients and quantum yields of products for reactions involving $O(^1D)$, $O_2(b^1\Sigma_g^+, v=0–2)$ and $O_2(a^1\Delta_g, v=0–5)$.

Reaction	Notation	Quantum yield, F	Rate coefficient Arrhenius form			Temperature range (K)	ξ	Reference
			A ($cm^3\ s^{-1}$)	n	b (K)			
$O(^1D)$ Reaction								
$O(^1D) + O(^3P) \rightarrow O(^3P) + O(^3P)$	$k(O(^1D); O(^3P))$		$2.2 \cdot 10^{-11}$			RT	0.27	[56]
$O(^1D) + O_2 \rightarrow O(^3P) + O_2(b^1\Sigma_g^+, v)$	$k(O(^1D); O_2)$		$3.95 \cdot 10^{-11}$			RT	0.08	[13]
$\rightarrow O(^3P) + O_2(a^1\Delta_g, v)$			$3.12 \cdot 10^{-11}$		55	104–354	0.08	[14]
			$3.10 \cdot 10^{-11}$		87	195–673	0.10	[58]
Quantum yield of products	$F(O(^1D) \rightarrow O_2\ (b, v=1); O_2)$	0.8				296–312	0.125	[57]
	$F(O(^1D) \rightarrow O_2(b, v=0); O_2)$	0.2[a]				296–312	0. 5[a]	
	$F(O(^1D) \rightarrow O_2(a, v=0); O_2)$	<0.05				RT		[13]
$O(^1D) + O_3 \rightarrow 2O_2 \rightarrow O_2 + 2O(^3P)$	$k(O(^1D);\ O_3)$		$2.4 \cdot 10^{-10}$			RT	0.20	[14]
$\rightarrow O_2 + O_2$						210–370	0.20	
Quantum yield of products	$F(O(^1D) \rightarrow O(^3P); O_3)$	0.5				RT		
$O(^1D) + N_2 \rightarrow O(^3P) + N_2(X^1\Sigma_g^+, v)$	$k(O(^1D); N_2)$		$3.10 \cdot 10^{-11}$			RT	0.10	[14]
			$2.15 \cdot 10^{-11}$		110	100–350	0.10	
			$2.20 \cdot 10^{-11}$		118	195–673	0.09	[58]
$O(^1D) + CO_2 \rightarrow CO + O_2$	$k(O(^1D); CO_2)$		$1.1 \cdot 10^{-10}$			RT	0.15	[14]
			$7.5 \cdot 10^{-11}$		115	200–350	0.15	
$O_2(b^1\Sigma_g^+, v=2)$ Reaction								
$O_2(b^1\Sigma_g^+, v'=2) + O(^3P) \rightarrow O_2(b^1\Sigma_g^+, v'') + O(^3P)$	$k(O_2(b, v=2); O(^3P))$		$1.07 \cdot 10^{-11}$			340–445	0.6	[30]
Quantum yield of products	$F(O_2(b, v=2) \rightarrow O_2(b, v=1);); O(^3P))$	0.5					0.8	
	$F(O_2(b, v=2) \rightarrow O_2(b, v=0);); O(^3P))$	0.5					0.8	
$O_2(b^1\Sigma_g^+, v=2) + O_2 \rightarrow O_2(X^3\Sigma_g^+, v=2) + O_2(b^1\Sigma_g^+, v=0)$	$k(O_2(b, v=2); O_2)$		$2.7 \cdot 10^{-12}$			RT	0.07	[28]
			$2.3 \cdot 10^{-11}$		−691	110–295	0.25	
			$3.15 \cdot 10^{-12}$			340–445	0.25	[30]
$O_2(b^1\Sigma_g^+, v=2) + O_3 \rightarrow 2O_2 + O(^3P)$	$k(O_2(b, v=2); O_3)$		$2.9 \cdot 10^{-10}$			340–445	0.4	[30]
$O_2(b^1\Sigma_g^+, v=2) + N_2 \rightarrow O_2(b^1\Sigma_g^+, v=0) + N_2(X^1\Sigma_g^+, v=1)$	$k(O_2(b, v=2); N_2)$		$<9 \cdot 10^{-13}$			RT		[28]
			$8.0 \cdot 10^{-15}$			110	0.40	
$O_2(b^1\Sigma_g^+, v=2) + CO_2 \rightarrow O_2(b^1\Sigma_g^+, v=1) + CO_2(100)$	$k(O_2(b, v=2); CO_2)$		$1.7 \cdot 10^{-12}$			RT	0.30	[28]
			$3.0 \cdot 10^{-12}$		−158	220–295	0.9	
$O_2(b^1\Sigma_g^+, v=1)$ Reaction								
$O_2(b^1\Sigma_g^+, v=1) + O(^3P) \rightarrow O_2 + O(^3P)$	$k(O_2(b, v=1); O(^3P))$		$4.5 \cdot 10^{-12}$			RT	0.18/−0.29	[57]
$O_2(b^1\Sigma_g^+, v=1) + O_2 \rightarrow O_2(X^3\Sigma_g^-, v=1) + O_2(b^1\Sigma_g^+, v=0)$	$k(O_2(b, v=1); O_2)$		$1.52 \cdot 10^{-11}$			RT	0.04	[57]
			$2.2 \cdot 10^{-11}$	1.0	−115	125–1000	0.40	
$O_2(b^1\Sigma_g^+, v=1) + O_3 \rightarrow 2O_2 + O(^3P)$	$k(O_2(b, v=1); O_3)$		$<3 \cdot 10^{-10}$			340–445		[30]
$O_2(b^1\Sigma_g^+, v=1) + N_2 \rightarrow O_2(b^1\Sigma_g^+, v=0) + N_2(X^1\Sigma_g^+, v=1)$	$k(O_2(b, v=1); N_2)$		$<7 \cdot 10^{-13}$			RT		[28]
$O_2(b^1\Sigma_g^+, v=1) + CO_2 \rightarrow O_2(b^1\Sigma_g^+, v=0) + CO_2(100)$	$k(O_2(b, v=1); CO_2)$		$<1.2 \cdot 10^{-12}$			RT		[28]
			$9 \cdot 10^{-13}$			220	0.6	
$O_2(b^1\Sigma_g^+, v=0)$ Reaction								
$O_2(b^1\Sigma_g^+, v=0) + O(^3P) \rightarrow O_2 + O(^3P)$	$k(O_2(b, v=0); O(^3P))$		$8 \cdot 10^{-14}$				4.0/−0.8[b]	[14]
$\rightarrow O_2(a^1\Delta_g, v) + O(^3P)$							0.25[b]	[13]

Table A1 (*continued*)

Reaction	Notation	Quantum yield, F	Rate coefficient Arrhenius form			Temperature range (K)	ξ	Reference
			A ($cm^3\ s^{-1}$)	n	b (K)			
Quantum yield of products	$F(O_2(b,v=0) \rightarrow O_2(a,v=0); O(^3P))$	0.75				RT		[59]
$O_2(b^1\Sigma_g^+, v=0) + O_2 \rightarrow O_2(a^1\Delta_g, v'=3\text{-}v'') + O_2(X^3\Sigma_g^-, v'')$	$k(O_2(b,v=0); O_2)$		$3.9 \cdot 10^{-17}$			RT	0.5	[14]
Quantum yield of products	$F(O_2(b,v=0) \rightarrow O_2(a,v=3); O_2)$	0.019				77		[31]
	$F(O_2(b,v=0) \rightarrow O_2(a,v=2); O_2)$	0.226						
	$F(O_2(b,v=0) \rightarrow O_2(a,v=1); O_2)$	0.525						
	$F(O_2(b,v=0) \rightarrow O_2(a,v=0); O_2)$	0.230						
$O_2(b^1\Sigma_g^+, v=0) + O_3 \rightarrow 2O_2 + O(^3P)$	$k(O_2(b,v=0); O_3)$		$2.2 \cdot 10^{-11}$			RT	0.15	[14]
$\rightarrow O_2(a^1\Delta_g, v) + O_3$			$3.5 \cdot 10^{-11}$		−135	210–370		
Quantum yield of products	$F(O_2(b,v=0) \rightarrow O(^3P); O_3)$	0.7				RT		
	$F(O_2(b,v=0) \rightarrow O_2(a,v); O_3)$	0.3				RT		
$O_2(b^1\Sigma_g^+, v=0) + N_2 \rightarrow$	$k(O_2(b,v=0); N_2)$		$2.1 \cdot 10^{-15}$			RT	0.10	[14]
$\rightarrow O_2(a^1\Delta_g, v=2) + N_2(X^1\Sigma_g^-, v=1)$			$1.8 \cdot 10^{-15}$		45	203–370		
$\rightarrow O_2(X^3\Sigma_g^+, v=9) + N_2(X^1\Sigma_g^+, v=0)$								
Quantum yield of products	$F(O_2(b,v=0) \rightarrow O_2(a,v=2);\ N_2)$	0.5				RT		[1]
	$F(O_2(b,v=0) \rightarrow O_2(X,v=9); N_2)$	0.5				RT		
$O_2(b^1\Sigma_g^+, v=0) + CO_2 \rightarrow O_2(a^1\Delta_g, v=0) + CO_2$	$k(O_2(b,v=0); CO_2)$		$4.2 \cdot 10^{-13}$			RT	0.20	[14]
			$4.2 \cdot 10^{-13}$			210–370		
Quantum yield of products	$F(O_2(b,v=0) \rightarrow O_2(a,v=0); CO_2)$	$\geqslant 0.9$				RT		
O_2 ($a^1\Delta_g$, $v > 2$) Reaction								
$O_2(a^1\Delta_g, v>2) + O(^3P) \rightarrow O_2 + O(^3P)$	$k(O_2(a,v>2); O(^3P))$		No data					[60]
$O_2(a^1\Delta_g, v>2) + O_2 \rightarrow O_2(X^3\Sigma_g^-, v) + O_2(a^1\Delta_g, v=0)$	$k(O_2(a,v>2); O_2)$		as $k(O_2(a,v=2); O_2)$					[1]
$O_2(a^1\Delta_g, v>2) + O_3 \rightarrow 2O_2 + O(^3P)$	$k(O_2(a,v>2); O_3)$		No data					
$O_2(a^1\Delta_g, v>2) + N_2 \rightarrow O_2 + N_2$	$k(O_2(a,v>2); N_2)$		as $k(O_2(a,v=2); N_2)$					[60]
$O_2(a^1\Delta_g, v>2) + CO_2 \rightarrow$ *products*	$k(O_2(a,v>2); CO_2)$		No data					[60]
O_2 ($a^1\Delta_g$, $v = 2$) Reaction								
$O_2(a^1\Delta_g, v=2) + O(^3P) \rightarrow O_2 + O(^3P)$	$k(O_2(a,v=2); O(^3P))$		No data					
$O_2(a^1\Delta_g, v=2) + O_2 \rightarrow O_2(X^3\Sigma_g^-, v=2) + O_2(a^1\Delta_g, v=0)$	$k(O_2(a,v=2); O_2)$		$3.6 \cdot 10^{-11}$			RT	0.11	[60]
$O_2(a^1\Delta_g, v=2) + O_3 \rightarrow 2O_2 + O(^3P)$	$k(O_2(a,v=2); O_3)$		No data					
$O_2(a^1\Delta_g, v=2) + N_2 \rightarrow O_2 + N_2$	$k(O_2(a,v=2); N_2)$		$<4 \cdot 10^{-15}$			RT		[60]
$O_2(a^1\Delta_g, v=2) + CO_2 \rightarrow$ *products*	$k(O_2(a,v=2); CO_2)$		No data					
O_2 ($a^1\Delta_g$, $v = 1$) Reaction								
$O_2(a^1\Delta_g, v=1) + O(^3P) \rightarrow O_2 + O(^3P)$	$k(O_2(a,v=1); O(^3P))$		$<4 \cdot 10^{-13}$			RT		[60]
$O_2(a^1\Delta_g, v=1) + O_2 \rightarrow O_2(X^3\Sigma_g^-, v=1) + O_2(a^1\Delta_g, v=0)$	$k(O_2(a,v=1); O_2)$		$5.6 \cdot 10^{-11}$			RT	0.20	[60]
$O_2(a^1\Delta_g, v=1) + O_3 \rightarrow 2O_2 + O(^3P)$	$k(O_2(a,v=1); O_3)$		$4.7 \cdot 10^{-12}$			RT	0.43	[23]
$O_2(a^1\Delta_g, v=1) + N_2 \rightarrow O_2 + N_2$	$k(O_2(a,v=1); N_2)$		$<3 \cdot 10^{-16}$			RT		[60]
$O_2(a^1\Delta_g, v=1) + CO_2 \rightarrow$ *products*	$k(O_2(a,v=1); CO_2)$		$1.5 \cdot 10^{-14}$			RT	0.13	[60]
			$1.2 \cdot 10^{-14}$			240	0.08	

(*continued on next page*)

Table A1 (*continued*)

Reaction	Notation	Quantum yield, F	Rate coefficient Arrhenius form			Temperature range (K)	ξ	Reference
			A ($cm^3\,s^{-1}$)	n	b (K)			
O_2 ($a^1\Delta_g$, v = 0) Reaction								
$O_2(a^1\Delta_g, v=0) + O(^3P) \rightarrow O_2 + O(^3P)$	$k(O_2(a,v=0);O(^3P))$		$<2\cdot10^{-16}$			RT		[14]
			$1\cdot10^{-16}$			RT	2.0/−0.7[c]	
$O_2(a^1\Delta_g, v=0) + O_2 \rightarrow O_2(X^3\Sigma_g^-, v'=5\text{-}v') + O_2(X^3\Sigma_g^-, v')$	$k(O_2(a,v=0);O_2)$		$1.7\cdot10^{-18}$			RT	0.20	[14]
			$3.6\cdot10^{-18}$		−220	100–450		
Quantum yield of products						77		[22]
	$F(O_2(a,v=0)\rightarrow O_2(X,v=5);O_2)$	0.014						
	$F(O_2(a,v=0)\rightarrow O_2(X,v=4);O_2)$	0.214						
	$F(O_2(a,v=0)\rightarrow O_2(X,v=3);O_2)$	0.772						
$O_2(a^1\Delta_g, v=0) + O^3 \rightarrow 2O_2 + O(^3P)$	$k(O_2(a,v=0);O_3)$		$3.8\cdot10^{-15}$			RT	0.25	[13]
			$5.2\cdot10^{-11}$		−2840	280–360		
$O_2(a^1\Delta_g, v=0) + N_2 \rightarrow O_2 + N_2$	$k(O_2(a,v=0);N_2)$		$\leqslant 1.4\cdot10^{-19}$					[13]
$O_2(a^1\Delta_g, v=0) + CO_2 \rightarrow products$	$k(O_2(a,v=0);CO_2)$		$\leqslant 2\cdot10^{-20}$					[13]

[a] The estimation of quantum yield $F(O(^1D) \rightarrow O_2(b,v=0);O_2) = 0.2 \pm 0.1$ is made by us basing on the statement of Pejakovic et al. [57] that during the experiment the nascent population of $O_2(b^1\Sigma_g^+, v=1)$ was nearly 4 times larger than that of $O_2(b^1\Sigma_g^+, v=0)$.

[b] There is an apparent contradiction between the estimations of the magnitude of uncertainty $k(O_2(b,v=0);O(^3P))$ in [13,14]. In any case, additional experimental studies are necessary, since this reaction is important (Sections 5.1 and 8.1).

[c] The recommendation of $k(O_2(a,v=0);O(^3P))$ value [14] is based on the upper limit of the rate coefficient reported by Clark and Wayne [61]. However, over the last decades, many authors used a value of the rate coefficient varying from $3\cdot10^{-16}$ to $5\cdot10^{-17}$ cm^3s^{-1} without any experimental verification. The contribution of this reaction is essential for the population kinetics of $O_2(a^1\Delta_g, v=0)$ as it was shown by the sensitivity analysis in this paper (Fig. 7, Table 8.1). Therefore, we suggest using the value $k(O_2(a,v=0);O(^3P)) \approx 1\cdot10^{-16}$ cm^3s^{-1} with a factor of uncertainty equal to 3 ($\boldsymbol{f}$ = 3, the corresponding values of ξ_{up} = 2.0 and ξ_{lo} = −0.7).

c. Absolute rate constant values k(RT) are given at room temperature (RT). It should be mentioned, that the authors used different values of RT, such as 292, 295, 298 or 300 K. The rate constants are given in units of concentration expressed as molecules per cubic centimetre and time in seconds. Only for reactions $O_2(b^1\Sigma_g^+, v=2) + O(^3P) \rightarrow O_2 + O(^3P)$ and $O_2(b^1\Sigma_g^+, v=2) + O_3 \rightarrow 2O_2 + O(^3P)$) there is no data obtained at room temperature, because the rate constants were measured in the temperature interval 340–445 K (experiment in stationary glow discharge in pure O_2 [30]).

d. The interpolations of experimental temperature dependences are expressed in generally accepted Arrhenius form, $k(T) = \boldsymbol{A}\cdot(T/292)^{\mathbf{n}}\cdot\exp(\boldsymbol{b}/T)$, where parameter $\boldsymbol{b}$ is expressed in Kelvins.

e. We indicate the temperature range of experimental data, where the values of parameters $\boldsymbol{A}$, $\mathbf{n}$ and $\boldsymbol{b}$ are valid. Typical temperature range is approximately 210–370 K. It should be noted that only for three reactions $O_2(b^1\Sigma_g^+, v=1) + O_2 \rightarrow O_2(X^3\Sigma_g^-, v=1) + O_2(b^1\Sigma_g^+, v=0)$, $O(^1D) + O_2 \rightarrow products$ and $O(^1D) + N_2 \rightarrow O(^3P) + N_2(X^1\Sigma_g^+, v)$ temperature range essentially exceeds this range, namely, it is from 125 to 1000 K for the first reaction and from 100 to 673 K for the remaining reactions.

f. For quantum yield of each C** in reaction A* + B → C** + D we use the notation $F(A^* \rightarrow C^{**};B)$, because in most reactions there are several product formation channels.

g. Relative uncertainties of k and F values as well as of $\boldsymbol{A}$ parameter are denoted as ξ. If the upper and lower boundaries of the relative uncertainty are different, we labelled them ξ_{up} and ξ_{lo}, respectively. In this case, we use the 'ξ_{up}/ξ_{lo}' notation in Table A1. If the uncertainties are symmetric, then we present only the absolute value of ξ. ξ_{up} and ξ_{lo} are connected with factor of uncertainty $\boldsymbol{f}$ used in [14] by equations $\xi_{up} = \boldsymbol{f} - 1$ and $\xi_{lo} = (1/\boldsymbol{f}) - 1$.

h. For some reactions involving the $O_2(a^1\Delta_g,\ v \geqslant 2)$ component, there is no data yet. Nevertheless, we present all possible reactions for the specious under consideration regardless of availability of experimental data. The sensitivity study shows that the contributions of these processes are insignificant in $O_2(a^1\Delta_g,\ v \geqslant 2)$ kinetics.

Appendix B

B.1. The system of kinetic equations for modelling the electronic-vibrational kinetics of excited oxygen molecules in the MLT region

In the framework of our model, we present the system of kinetic equations for 10 excited species $O(^1D)$, $O_2(b^1\Sigma_g^+, v=0,1,2)$ and $O_2(a^1\Delta_g, v=0\text{–}5)$. Yankovsky and Manuilova [1] introduced all photoprocesses necessary for YM2011 model (see Table B2), and the methods of calculation of the rates of these photoprocesses were described in [11].

In all kinetic equations, the same type of quenching factor is presented:

$$Q(x_i) = A_i + [O_2]\cdot k(x_i;O_2) + [O(^3P)]\cdot k(x_i;O(^3P)) + [O_3] \cdot k(x_i;O_3) + [N_2]\cdot k(x_i;N_2) + [CO_2]\cdot k(x_i;CO_2), \quad (B.1)$$

where x_i is the excited level of the corresponding component, A_i – Einstein coefficient, $k(x_i;y_j)$ – the rate coefficient of the quenching reaction of x_i in collision with y_j (see Appendix A). In this study x_i are $O(^1D)$, $O_2(b^1\Sigma_g^+, v=0,1,2)$ and $O_2(a^1\Delta_g, v=0\text{–}5)$; y_j are O_2, O (^3P), N_2, O_3 and CO_2.

Table B1
The system of kinetic equations for excited species.

1. $\mathbf{O(^1D)}$

$$\frac{\partial[O(^1D)]}{\partial t} = [O_2] * \left(J_{SRC} + J_{Ly\,\alpha} * F(Ly\ \alpha \rightarrow O(^1D))\right) + [O_3] * J_{HB} * F(HB \rightarrow O(^1D)) - [O(^1D)] * Q(O(^1D))$$

2. $\mathbf{O_2\left(b^1\Sigma_g^+, v=2\right)}$

$$\frac{\partial[O_2(b^1\Sigma_g^+, v=2)]}{\partial t} = [O_2] * g_\gamma - \left[O_2\left(b^1\Sigma_g^+, v=2\right)\right] * Q\left(O_2\left(b^1\Sigma_g^+, v=2\right)\right)$$

3. $\mathbf{O_2\left(b^1\Sigma_g^+, v=1\right)}$

$$\frac{\partial[O_2(b^1\Sigma_g^+, v=1)]}{\partial t} = [O_2] * g_\beta + [O(^1D)] * [O_2] * k(O(^1D); O_2) * F(O(^1D) \rightarrow O_2(b, v=1); O_2) + [O_2\left(b^1\Sigma_g^+, v=2\right)] * [O] * k(O_2(b, v=2); O) * F(O_2(b, v=2) \rightarrow O_2(b, v=1); O))$$
$$- \left[O_2\left(b^1\Sigma_g^+, v=1\right)\right] * Q\left(O_2\left(b^1\Sigma_g^+, v=1\right)\right)$$

4. $\mathbf{O_2\left(b^1\Sigma_g^+, v=0\right)}$

$$\frac{\partial[O_2(b^1\Sigma_g^+, v=0)]}{\partial t} = [O_2] * g_\alpha + [O(^1D)] * [O_2] * k(O(^1D); O_2) * F(O(^1D) \rightarrow O_2(b, v=0); O_2)$$
$$+ \left[O_2\left(b^1\Sigma_g^+, v=1\right)\right] * ([O_2] * k(O_2(b, v=1); O_2) + [O] * k(O_2(b, v=1); O)) + \left[O_2\left(b^1\Sigma_g^+, v=2\right)\right] * ([O_2] * k(O_2(b, v=2); O_2)$$
$$+ [O] * k(O_2(b, v=2); O) * F(O_2(b, v=2) \rightarrow O_2(b, v=0); O)) - \left[O_2\left(b^1\Sigma_g^+, v=0\right)\right] * Q\left(O_2\left(b^1\Sigma_g^+, v=0\right)\right)$$

5. $\mathbf{O_2\left(a^1\Delta_g, v=5\right)}$

$$\frac{\partial[O_2(a^1\Delta_g, v=5)]}{\partial t} = [O_3] * J_{HB} * F(HB \rightarrow O_2(a^1\Delta_g, v=5)) - [O_2(a^1\Delta_g, v=5)] * Q(O_2(a^1\Delta_g, v=5))$$

6. $\mathbf{O_2\left(a^1\Delta_g, v=4\right)}$

$$\frac{\partial[O_2(a^1\Delta_g, v=4)]}{\partial t} = [O_3] * J_{HB} * F(HB \rightarrow O_2(a^1\Delta_g, v=4)) - [O_2(a^1\Delta_g, v=4)] * Q(O_2(a^1\Delta_g, v=4))$$

7. $\mathbf{O_2\left(a^1\Delta_g, v=3\right)}$

$$\frac{\partial[O_2(a^1\Delta_g, v=3)]}{\partial t} = [O_3] * J_{HB} * F(HB \rightarrow O_2(a^1\Delta_g, v=3)) + \left[O_2\left(b^1\Sigma_g^+, v=0\right)\right] * [O_2] * k(O_2(b, v=0); O_2) * F(O_2(b, v=0) \rightarrow O_2(a, v=3); O_2)$$
$$- [O_2(a^1\Delta_g, v=3)] * Q(O_2(a^1\Delta_g, v=3))$$

8. $\mathbf{O_2\left(a^1\Delta_g, v=2\right)}$

$$\frac{\partial[O_2(a^1\Delta_g, v=2)]}{\partial t} = [O_3] * J_{HB} * F(HB \rightarrow O_2(a^1\Delta_g, v=2)) + \left[O_2\left(b^1\Sigma_g^+, v=0\right)\right] * [N_2] * k(O_2(b, v=0); N_2) * F(O_2(b, v=0) \rightarrow O_2(a, v=2); N_2)$$
$$+ \left[O_2\left(b^1\Sigma_g^+, v=0\right)\right] * [O_2] * k(O_2(b, v=0); O_2) * F(O_2(b, v=0) \rightarrow O_2(a, v=2); O_2) - [O_2(a^1\Delta_g, v=2)] * Q(O_2(a^1\Delta_g, v=2))$$

9. $\mathbf{O_2\left(a^1\Delta_g, v=1\right)}$

$$\frac{\partial[O_2(a^1\Delta_g, v=1)]}{\partial t} = [O_3] * J_{HB} * F(HB \rightarrow O_2(a^1\Delta_g, v=1)) + \left[O_2\left(b^1\Sigma_g^+, v=0\right)\right] * [O_2] * k(O_2(b, v=0); O_2) * F(O_2(b, v=0) \rightarrow O_2(a, v=1); O_2)$$
$$+ [O_2(a, v=2)] * [O_2] * k(O_2(a, v=2); O_2) - [O_2(a^1\Delta_g, v=1)] * Q(O_2(a^1\Delta_g, v=1))$$

10. $\mathbf{O_2\left(a^1\Delta_g, v=0\right)}$

$$\frac{\partial[O_2(a^1\Delta_g, v=0)]}{\partial t} = [O_3] * J_{HB} * F(HB \rightarrow O_2(a^1\Delta_g, v=0)) + [O_2] * g_{IRa} + [O_2(a^1\Delta_g, v=1)] * [N_2] * k(O_2(a, v=1); N_2)$$
$$+ \sum_{v=1}^{5} \left([O_2(a^1\Delta_g, v)] * [O_2] * k(O_2(a, v); O_2)\right) + \left[O_2\left(b^1\Sigma_g^+, v=0\right)\right] * \{[O_2] * k(O_2(b, v=0); O_2) * F(O_2(b, v=0)$$
$$\rightarrow O_2(a, v=0); O_2) + [O] * k(O_2(b, v=0); O) * F(O_2(b, v=0) \rightarrow O_2(a, v=0); O) + [O_3] * k(O_2(b, v=0); O_3) * F(O_2(b, v=0) \rightarrow O_2(a, v=0); O_3)$$
$$+ [CO_2] * k(O_2(b, v=0); CO_2) * F(O_2(b, v=0) \rightarrow O_2(a, v=0); CO_2)\} - [O_2(a^1\Delta_g, v=0)] * Q(O_2(a^1\Delta_g, v=0))$$

It should be noted that the system of kinetic equations for 10 excited species is nonlinear because the most part of the model parameters (e.g. temperature, the main atmospheric components concentrations, array of rate coefficients) take part in the processes of excitation as well as in quenching processes of the excited species (the target functions).

Table B2
The photoprocesses included into the kinetic equations.

Photoprocesses	Rate coefficients and Einstein coefficients, s^{-1}	Quantum yield of product
$O_2 + h\nu$(Schumann-Runge continuum) $\rightarrow O(^1D) + O(^3P)$	J_{SRC}	$F(SRC \rightarrow O(^1D))$
$O_2 + h\nu$(H Lyman α line) $\rightarrow O(^1D) + O(^3P)$	$J_{Ly\,\alpha}$	$F(Ly\ \alpha)$
$O_2 + h\nu$(762 nm band) $\rightarrow O_2(b^1\Sigma_g^+, v = 0)$	g_α	
$O_2 + h\nu$(688 nm band) $\rightarrow O_2(b^1\Sigma_g^+, v = 1)$	g_β	
$O_2 + h\nu$(629 nm band) $\rightarrow O_2(b^1\Sigma_g^+, v = 2)$	g_γ	
$O_2 + h\nu$(1.27 μm band) $\rightarrow O_2(a^1\Delta_g, v = 0)$	g_{IRa}	
$O_3 + h\nu$(Hartley band) $\rightarrow O_2(a^1\Delta_g, v) + O(^1D)$	J_{HB}	$F(HB \rightarrow O(^1D))$ $F(HB \rightarrow O_2(a^1\Delta_g, v))$[a]
$O(^1D_2) \rightarrow O(^3P_{0,1,2}) + h\nu(630.0, 636.4$ and 639.2 nm lines)	A_D	$9 \cdot 10^{-3}\ s^{-1}$
$O_2(b^1\Sigma_g^+, v') \rightarrow O_2(X^3\Sigma_g^-, v'') + h\nu(O_2$ Atm bands$(v', v''))$	$A_{b,v'\rightarrow X,v''}$	See Table 7.1
$O_2(a^1\Delta_g, v') \rightarrow O_2(X^3\Sigma_g^-, v'') + h\nu(O_2$ IR Atm bands$(v', v''))$	$A_{a,v'\rightarrow X,v''}$	

[a] Analytical interpolated formulae of the quantum yields of the molecules $O_2(a^1\Delta_g, v = 0–5)$ depending on vibrational number, v, and on wavelength at ozone photolysis in Hartley band (in 200–320 nm range) were deduced in [11,12].

Appendix C

C.1. Analytical expressions of sensitivity coefficients for forward and inverse problems in framework YM2011 model

Simplified notations (in this section): $O_2(b, 1) = O_2(b^1\Sigma_g^+, v = 1)$; $O_2(b, 2) = O_2(b^1\Sigma_g^+, v = 2)$. Rate coefficient k_{y_j} corresponds to reaction $O_2(b^1\Sigma_g^+, v = 1) + y_j \rightarrow$ *products*, where $y_j = O(^3P)$, O_2 or CO_2; the notations of rate coefficients $k_{y_j}^D$ or $k_{y_j}^{b2}$ are used for reactions $O(^1D) + y_j \rightarrow$ *products* and $O_2(b^1\Sigma_g^+, v = 2) + y_j \rightarrow$ *products*, correspondingly. The only exception is made for the main reaction of the energy transfer of YM2011 model: $O(^1D) + O_2 \rightarrow O(^3P) + O_2(b^1\Sigma_g^+, v)$, for which the rate coefficient is designated as $k_{O(1D)+O2}$. The quantum yield of $O_2(b^1\Sigma_g^+, v = 1)$ in this reaction is designated as $\Psi = F(O(^1D) \rightarrow O_2(b^1\Sigma_g^+,\ v = 1); O_2)$. Rates of $O(^1D)$ production in photolysis of O_2 in the H Lyman-α line and photolysis of O_3 in the Hartley band are designated as $\Theta_L = J_{Ly\,\alpha} \cdot F(Ly\ \alpha)$ and $\chi = J_{HB} \cdot F(HB \rightarrow O(^1D))$, correspondingly. Parameters of temperature dependences $\boldsymbol{b}_1$, $\boldsymbol{b}_2$ and $\boldsymbol{b}_3$ for the rate coefficients of reactions are given in Table A1 (Appendix A):

Table C1
Forward problem: calculation of altitude profile of $[O_2(b^1\Sigma_g^+, v = 1)]$.

Parameter, z_i	Sensitivity coefficient for forward problem, $S(O_2(b^1\Sigma_g^+, v = 1); z_i)$	
$O_2(b^1\Sigma_g^+, v = 2)$	$\frac{g_\gamma \cdot [O(^3P)] \cdot [O_2] \cdot k_{O(^3P)}^{b2} \cdot F(O_2(b,2) \rightarrow O_2(b,1); O(^3P))}{[O_2(b,1)] \cdot Q(O_2(b,1)) \cdot Q(O_2(b,2))}$	
$O(^3P)$	$\frac{[O(^3P)] \cdot k_{O(^3P)}^D}{Q(O(^1D))} \cdot \left(\frac{[O_2] \cdot g_\beta}{[O_2(b,1)] \cdot Q(O_2(b,1))} - 1\right) - \frac{[O(^3P)] \cdot k_{O(^3P)}}{Q(O_2(b,1))}$	
O_2	$1 + [O_2] \cdot \left\{\frac{k_{O(1D)+O2} \cdot (g_\beta + J_{SRC} + \Theta_L) \cdot \Psi)}{[O_2(b,1)] \cdot Q(O_2(b,1)) \cdot Q(O(^1D)} - \frac{k_{O2}}{Q(O_2(b,1))} - \frac{k_{O(1D)+O2}}{Q(O(^1D))}\right\}$	
O_3	$\frac{[O_2] \cdot k_{O(1D)+O2} \cdot \Psi \cdot [O_3] \cdot \chi}{[O_2(b, v=1)] \cdot Q(O_2(b,1)) \cdot Q(O(^1D))}$	
N_2	$\frac{[N_2] \cdot k_{N2}^D}{Q(O(^1D))} \cdot \left(\frac{[O_2] \cdot g_\beta}{[O_2(b,1)] \cdot Q(O_2(b,1))} - 1\right) - \frac{[N_2] \cdot k_{N2}}{Q(O_2(b,1))}$	
CO_2	$\frac{[CO_2] \cdot k_{CO2}^D}{Q(O(^1D))} \cdot \left(\frac{[O_2] \cdot g_\beta}{[O_2(b,1)] \cdot Q(O_2(b,1))} - 1\right) - \frac{[CO_2] \cdot k_{CO2}}{Q(O_2(b,1))}$	
T	$\left\{\left(1 - \frac{[O_2] \cdot k_{O(1D)+O2}}{Q(O(^1D))}\right) \cdot \left(\frac{b_1}{T}\right) - \frac{[N_2] \cdot k_{N2}^D}{Q(O(^1D))} \cdot \left(\frac{b_2}{T}\right)\right\} \cdot \left(\frac{[O_2] \cdot g_\beta}{[O_2(b,1)] \cdot Q(O_2(b,1))} - 1\right) + \frac{[O_2] \cdot k_{O2}}{Q(O_2(b,1))} \cdot \left(\frac{b_3}{T} - 1\right)$	
J_{HB}	$\frac{[O_3] \cdot \chi \cdot [O_2] \cdot k_{O(1D)+O2} \cdot \Psi}{[O_2(b,1)] \cdot Q(O_2(b,1)) \cdot Q(O(^1D))}$	
J_{SRC}	$\frac{[O_2] \cdot J_{SRC} \cdot [O_2] \cdot k_{O(1D)+O2} \cdot \Psi}{[O_2(b,1)] \cdot Q(O_2(b,1)) \cdot Q(O(^1D))}$	
$J_{Ly\,\alpha} \cdot F(Ly\ \alpha)$	$\frac{[O_2] \cdot \Theta_L \cdot [O_2] \cdot k_{O(1D)+O2} \cdot \Psi}{[O_2(b,1)] \cdot Q(O_2(b,1)) \cdot Q(O(^1D))}$	
g_β	$\frac{[O_2] \cdot g_\beta}{[O_2(b,1)] \cdot Q(O_2(b,1))}$	
$A_{O(1D)}$	$-\frac{A_{O(1D)}}{Q(O(^1D))}$	
$k(O(^1D); y_j)$	$\frac{[y_j] \cdot k_{y_j}^D}{Q(O(^1D))} \cdot \left(\frac{[O_2] \cdot g_\beta}{[O_2(b,1)] \cdot Q(O_2(b,1))} - 1\right)$	where $y_j = O(^3P)$, O_3, N_2, CO_2
$k(O(^1D); O_2)$	$\left(1 - \frac{[O_2] \cdot k_{O(1D)+O2}}{Q(O(^1D))}\right) \cdot \left(\frac{[O_2] \cdot g_\beta}{[O_2(b,1)] \cdot Q(O_2(b,1))} - 1\right)$	
Ψ	$1 - \frac{[O_2] \cdot g_\beta}{[O_2(b,1)] \cdot Q(O_2(b,1))}$	
$A_{O2(b,\,v=1)}$	$-\frac{A_{O2(b,\,v=1)}}{Q(O_2(b,1))}$	
$k(O_2(b^1\Sigma_g^+, v = 1); y_j)$	$-\frac{[y_j] \cdot k_{y_j}}{Q(O_2(b,1))}$	where $y_j = O(^3P)$, O_2, CO_2

Table C2
Inverse problem: retrieval of $[O(^3P)]$ altitude profile from $[O_2(b^1\Sigma_g^+, v=1)]$.

Parameter, z_i	Sensitivity coefficient for inverse problem, $S_{O2(b,v=1)}(O(^3P); z_i)$	
$O(^3P)$	–	
O_2	$1+\frac{A_{O_2(b,v=1)}\cdot Q(O(^1D))+[N_2]\cdot k^D_{N2}\cdot Q(O_2(b,1))}{Q(O(^1D))\cdot[O(^3P)]\cdot k_{O(3P)}+Q(O_2(b,1))\cdot[O(^3P)]\cdot k^D_{O(3P)}}$	
O_3	$\left(\left(\frac{[O(^3P)]\cdot k^D_{O(3P)}}{Q(O(^1D))}\right)\cdot\left(1+\frac{[O_2]\cdot(J_{SRC}+\Theta_L)}{[O_3]\cdot\chi}\right)+\frac{[O_2(b,v=1)]\cdot[O(^3P)]\cdot k_{O(3P)}\cdot Q(O(^1D))}{[O_2]\cdot k_{O(1D)+O2}\cdot\Psi\cdot[O_3]\cdot\chi}\cdot\right)^{-1}$	
N_2	$-\frac{[N_2]}{[O(^3P)]}\cdot\frac{Q(O_2(b,1))\cdot k^D_{N2}+Q(O(^1D))\cdot k_{N2}}{Q(O_2(b,1))\cdot k^D_{O(3P)}+Q(O(^1D))\cdot k_{O(3P)}}$	
CO_2	$\frac{[CO_2]}{[O(^3P)]}\cdot\frac{[O_2(b,1)]\cdot(Q(O(^1D))\cdot k_{CO2}-Q(O_2(b,1))\cdot k^D_{CO2})+[O_2]\cdot g_\beta\cdot k^D_{CO2}}{[O_2(b,1)]\cdot(Q(O(^1D))\cdot k_{O(3P)}+Q(O_2(b,1))\cdot k^D_{O(3P)})-[O_2]\cdot g_\beta\cdot k^D_{O(3P)}}$	
T	$\left\{\left(\frac{b_1}{T}\right)\cdot\left(\frac{[O_2]\cdot k_{O(1D)+O2}}{Q(O(^1D))}-1\right)+\left(\frac{b_2}{T}\right)\cdot\frac{[N_2]\cdot k^D_{N2}}{Q(O(^1D))}+\frac{Q(O(^1D))\cdot[O_2(b,1)]\cdot[O_2]\cdot k_{O2}}{[O_2]^2\cdot k_{O(1D)+O2}\cdot(J_{SRC}+\Theta_L)\cdot\Psi}\cdot\left(\frac{b_3}{T}-1\right)\right\}$ / $\left(\left[O(^3P)\right]\cdot\left(\frac{k^D_{O(3P)}}{Q(O(^1D))}+\frac{k_{O(3P)}\cdot Q(O(^1D))\cdot[O_2(b,1)]}{[O_2]^2\cdot k_{O(1D)+O2}\cdot(J_{SRC}+\Theta_L)\cdot\Psi}\right)\right)$	
$J_{HB}\cdot F(HB\rightarrow O(^1D))$	$\frac{1}{\left(\frac{[O(^3P)]\cdot k^D_{O(3P)}}{Q(O(^1D))}\right)\cdot\left(1+\frac{[O_2]\cdot(J_{SRC}+\Theta_L)}{[O_3]\cdot\chi}\right)+\frac{[O_2(b,1)]\cdot[O(^3P)]\cdot k_{O(3P)}\cdot Q(O(^1D))}{[O_2]\cdot k_{O(1D)+O2}\cdot\Psi\cdot[O_3]\cdot\chi}}$	
J_{SRC}	$\frac{1}{\left(1+\frac{[O_3]\cdot\chi}{[O_2]\cdot J_{SRC}}\right)\frac{[O(^3P)]\cdot k^D_{O(3P)}}{Q(O(^1D))}+\frac{[O_2(b,1)]\cdot[O(^3P)]\cdot k_{O(3P)}\cdot Q(O(^1D))}{[O_2]\cdot k_{O(1D)+O2}\cdot[O_2]\cdot J_{SRC}\cdot\Psi}}$	
$J_{Ly\,\alpha}\cdot F(Ly\ \alpha)$	$\frac{1}{\left(1+\frac{[O_3]\cdot\chi}{[O_2]\cdot\Theta_L}\right)\frac{[O(^3P)]\cdot k^D_{O(3P)}}{Q(O(^1D))}+\frac{[O_2(b,1)]\cdot[O(^3P)]\cdot k_{O(3P)}\cdot Q(O(^1D))}{[O_2]\cdot k_{O(1D)+O2}\cdot[O_2]\cdot\Theta_L\cdot\Psi}}$	
g_β	$\frac{1}{\frac{[O_2(b,1)]\cdot[O(^3P)]\cdot Q(O_2(b,1))}{[O_2]\cdot g_\beta}\left(\frac{k_{O(3P)}}{Q(O_2(b,1))}+\frac{k^D_{O(3P)}}{Q(O(^1D))}\right)-\frac{[O(^3P)]\cdot k^D_{O(3P)}}{Q(O(^1D))}}$	
$k(O(^1D); y_j)$	$\frac{-[y_j]\cdot k^D_{y_j}\cdot Q(O_2(b,1))}{[O(^3P)]\cdot(k_{O(3P)}\cdot Q(O(^1D))+k^D_{O(3P)}\cdot Q(O_2(b,1)))}$	where $y_j = O(^3P)$, O_3, N_2, CO_2
$k(O(^1D); O_2)$	$\frac{Q(O_2(b,1))\cdot(Q(O(^1D))-[O_2]\cdot k_{O(1D)+O2})}{[O(^3P)]\cdot(Q(O(^1D))\cdot k_{O(3P)}+Q(O_2(b,1))\cdot k^D_{O(3P)})}$	
Ψ	$\left(\frac{[O(^3P)]\cdot k^D_{O(3P)}}{Q(O(^1D))}+\frac{[O(^3P)]\cdot k_{O(3P)}\cdot[O_2(b,1)]}{[O_2(b,1)]\cdot Q(O_2(b,1))-[O_2]\cdot g_\beta}\right)^{-1}$	
$A_{O2(b,v=1)}$	$-\frac{A_{O_2(b,v=1)}}{Q(O_2(b,v=1))}\cdot\frac{1}{\frac{[O(^3P)]\cdot k_{O(3P)}}{Q(O_2(b,1))}+\frac{[O(^3P)]\cdot k^D_{O(3P)}}{Q(O(^1D))}\left(1-\frac{[O_2]\cdot g_\beta}{[O_2(b,1)]\cdot Q(O_2(b,1))}\right)}$	
$k(O_2(b^1\Sigma_g^+, v=1); y_j)$	$\frac{-[y_j]\cdot k_{y_j}\cdot Q(O(^1D))}{[O(^3P)]\cdot(k_{O(3P)}\cdot Q(O(^1D))+k^D_{O(3P)}\cdot Q(O_2(b,1)))}$	where $y_j = O(^3P)$, O_2, CO_2

Table C3
Inverse problem: retrieval of $[O_3]$ altitude profile from $[O_2(b^1\Sigma_g^+, v=1)]$.

Parameter, z_i	Sensitivity coefficient for inverse problem, $S_{O2(b,v=1)}(O_3; z_i)$	
$O(^3P)$	$\frac{[O(^3P)]\cdot k^D_{O(3P)}}{Q(O(^1D))}\cdot\left(1+\frac{[O_2]\cdot(J_{SRC}+\Theta_L)}{[O_3]\cdot\chi}\right)+\frac{[O(^3P)]\cdot([O_2(b,1)]\cdot k_{O(3P)}\cdot Q(O(^1D)}{[O_2]\cdot k_{O(1D)+O2}\cdot\Psi\cdot[O_3]\cdot\chi}$	
O_2	$1-\left(1+\frac{[O_2]\cdot(J_{SRC}+\Theta_L)}{[O_3]\cdot\chi}\right)\cdot\frac{[N_2]\cdot k^D_{N2}}{Q(O(^1D))}$	
O_3	–	
N_2	$\frac{[N_2]\cdot k^D_{N2}}{Q(O(^1D))}\cdot\left(1+\frac{[O_2]\cdot(J_{SRC}+\Theta_L)}{[O_3]\cdot\chi}\right)$	
CO_2	$\frac{[CO_2]\cdot k^D_{CO2}}{Q(O(^1D))}\cdot\left(1+\frac{[O_2]\cdot(J_{SRC}+\Theta_L)}{[O_3]\cdot\chi}\right)+\frac{[CO_2]\cdot k_{CO2}\cdot[O_2(b,1)]\cdot Q(O(^1D))}{[O_3]\cdot\chi\cdot[O_2]\cdot k_{O(1D)+O2}\cdot\Psi}$	
T	$\left(1+\frac{[O_2]\cdot(J_{SRC}+\Theta_L)}{[O_3]\cdot\chi}\right)\cdot\left\{\left(\frac{b_1}{T}\right)\cdot\left(1-\frac{[O_2]\cdot k_{O(1D)+O2}}{Q(O(^1D))}\right)-\left(\frac{b_2}{T}\right)\cdot\left(\frac{[N_2]\cdot k^D_{N2}}{Q(O(^1D))}\right)\right\}+\left(1-\frac{b_3}{T}\right)\cdot\left(\frac{[O_2(b,v=1)]\cdot Q(O(^1D))\cdot k_{O2}}{[O_2]\cdot k_{O(1D)+O2}\cdot\Psi\cdot[O_3]\cdot\chi}\right)$	
$J_{HB}\cdot F(HB\rightarrow O(^1D))$	-1	
J_{SRC}	$-\frac{[O_2]\cdot J_{SRC}}{[O_3]\cdot\chi}$	
$J_{Ly\,\alpha}\cdot F(Ly\ \alpha)$	$-\frac{[O_2]\cdot\Theta_L}{[O_3]\cdot\chi}$	
g_β	$-\frac{[O_2]\cdot g_\beta\cdot Q(O(^1D))}{[O_2]\cdot k_{O(1D)+O2}\cdot\Psi\cdot[O_3]\cdot\chi}$	
$k(O(^1D); y_j)$	$\frac{[y_j]\cdot k^D_{y_j}}{Q(O(^1D))}\cdot\left(1+\frac{[O_2]\cdot(J_{SRC}+\Theta_L)}{[O_3]\cdot\chi}\right)$	where $y_j = O(^3P)$, O_3, N_2, CO_2
$k(O(^1D); O_2)$	$\left(1-\frac{[O_2]\cdot k_{O(1D)+O2}}{Q(O(^1D))}\right)\cdot\left(1+\frac{[O_2]\cdot(J_{SRC}+\Theta_L)}{[O_3]\cdot\chi}\right)$	
Ψ	$-1-\frac{[O_2]\cdot(J_{SRC}+\Theta_L)}{[O_3]\cdot\chi}$	
$A_{O2(b,v=1)}$	$\frac{A_{O2(b,v=1)}\cdot[O_2(b,1)]\cdot Q(O(^1D))}{[O_2]\cdot k_{O(1D)+O2}\cdot\Psi\cdot[O_3]\cdot\chi}$	
$k(O_2(b^1\Sigma_g^+, v=1); y_j)$	$-\frac{[O_2(b,1)]\cdot Q(O(^1D))\cdot[y_j]\cdot k_{y_j}}{[O_2]\cdot k_{O(1D)+O2}\cdot\Psi\cdot[O_3]\cdot\chi}$	where $y_j = O(^3P)$, O_2, CO_2

$$O(^1D)+O_2\rightarrow products,\ k(O(^1D);O_2)=3.1\cdot10^{-11}\cdot\exp(\boldsymbol{b}_1/T);$$

$$O(^1D)+N_2\rightarrow products,\ k(O(^1D);N_2)=2.2\cdot10^{-11}\cdot\exp(\boldsymbol{b}_2/T);$$

$$O_2(b^1\Sigma_g^+,\ v=1)+O_2\rightarrow products,\ k(O_2(b^1\Sigma_g^+,\ v=1);O_2)$$
$$=2.2\cdot10^{-11}\cdot(T/292)\cdot\exp(\boldsymbol{b}_3/T).$$

References

[1] V.A. Yankovsky, R.O. Manuilova, Model of daytime emissions of electronically–vibrationally excited products of O_3 and O_2 photolysis: application to ozone retrieval, Ann. Geophys. 24 (11) (2006) 2823–2839, http://dx.doi.org/10.5194/angeo-24-2823-2006.

[2] A.G. Feofilov, A.A. Kutepov, Infrared radiation in the mesosphere and lower thermosphere: energetic effects and remote sensing, Surv. Geophys. 33 (2012) 1231–1280, http://dx.doi.org/10.1007/s10712-012-9204-0.

[3] A.G. Feofilov, A.A. Kutepov, C.-Y. She, A.K. Smith, W.D. Pesnell, R.A. Goldberg, CO_2(v2)–O quenching rate coefficient derived from coincidental SABER/TIMED and Fort Collins lidar observations of the mesosphere and lower thermosphere, Atmos. Chem. Phys. 12 (2012) 9013–9023, http://dx.doi.org/10.5194/acp-12-9013-2012.

[4] R. Sharma, Technical note: on the possibly missing mechanism of 15 μm emission in the mesosphere–lower thermosphere (MLT), Atmos. Chem. Phys. 15 (2015) 1661–1667, http://dx.doi.org/10.5194/acp-15-1661-2015.

[5] S.W. Bougher, D.M. Hunten, R.G. Roble, CO_2 cooling in terrestrial planet thermospheres, J. Geophys. Res. 99 (1994) 14609–14622, http://dx.doi.org/10.1007/BF00613287.

[6] A.K. Smith, V.L. Harvey, M.G. Mlynczak, B. Funke, M. Garcia-Comas, M. Kaufmann, E. Kyrölä, M. López-Puertas, I. McDade, C.E. Randall, J.M. Russell III, P.E. Sheese, M. Shiotani, W.R. Skinner, M. Suzuki, K.A. Walker, Satellite observations of ozone in the upper mesosphere, J. Geophys. Res. D 118 (2013) 5803–5821, http://dx.doi.org/10.1002/jgrd.50445.

[7] M.G. Mlynczak, L.A. Hunt, J.C. Mast, B.T. Marshall, J.M. Russell III, A.K. Smith, D. E. Siskind, J.-H. Yee, C.J. Mertens, F.J. Martin-Torres, R.E. Thompson, D.P. Drob, L.L. Gordley, Atomic oxygen in the mesosphere and lower thermosphere derived from SABER: algorithm theoretical basis and measurement uncertainty, J. Geophys. Res. A 118 (2013) 5724–5735, http://dx.doi.org/10.1002/jgrd.50401.

[8] V.A. Yankovsky, R.O. Manuilova, A.S. Babaev, A.G. Feofilov, A.A. Kutepov, Model of electronic-vibrational kinetics of the O_3 and O_2 photolysis products in the middle atmosphere: applications to water vapour retrievals from SABER/TIMED 6.3 μm radiance measurements, Int. J. Remote Sens. 33 (2011) 3065–3078, http://dx.doi.org/10.1080/01431161.2010.541506.

[9] V.A. Yankovsky, A.S. Babaev, Photolysis of O_3 at Hartley, Chappuis, Huggins, and Wulf bands in the middle atmosphere: vibrational kinetics of oxygen molecules $O_2(X^3\Sigma_g^-, v\leqslant 35)$, Atmos. Ocean. Opt. 24 (2011) 6–16, http://dx.doi.org/10.1134/S1024856011010155.

[10] V.A. Yankovsky, R.O. Manuilova, V.A. Kuleshova, Heating of the middle atmosphere as a result of quenching of the products of O_2 and O_3 photodissociation, SPIE Proc. – Int. Soc. Opt. Eng. (USA) 5743 (2004) 34–40, http://dx.doi.org/10.1117/12.606261.

[11] V.A. Yankovsky, V.A. Kuleshova, R.O. Manuilova, A.O. Semenov, Retrieval of total ozone in the mesosphere with a new model of electronic-vibrational kinetics of O_2 and O_3 photolysis products, Izvestiya, Atmos. Ocean. Phys. 43 (2007) 514–525, http://dx.doi.org/10.1134/S0001433807040135.

[12] V.A. Yankovsky, V.A. Kuleshova, Ozone photodissociation at excitation within the Hartley absorption band. Analytical description of quantum yields $O_2(a^1\Delta_g, v=0–3)$ depending on the wavelength, Atmos. Ocean. Opt. 19 (2006) 514–518. ISSN: 1024-8560 (Print) 2070-0393 (Online).

[13] R. Atkinson, D.L. Baulch, R.A. Cox, J.N. Crowley, R.F. Hampson, R.G. Hynes, M.E. Jenkin, M.J. Rossi, J. Troe, Evaluated kinetic and photochemical data for atmospheric chemistry: volume I – gas phase reactions of O_x, HO_x, No_x and SO_x species, Atmos. Chem. Phys. 4 (2004) 1461–1738, http://dx.doi.org/10.5194/acp-4-1461-2004.

[14] S.P. Sander, R.R. Friedl, J.P.D. Abbatt, J.R. Barker, J.B. Burkholder, D.M. Golden, C. E. Kolb, M.J. Kurylo, G.K. Moortgat, P.H. Wine, R.E. Huie, V.L. Orkin, Chemical Kinetics and Photochemical Data for Use in Atmospheric Studies, JPL Publication 10-6, Evaluation Number 17, California Institute of Technology, Pasadena, California, 2011.

[15] M. Gauthier, D.R. Snelling, Production de $O_2(b^1\Sigma_g^+, v=0,1,2)$ par la reaction $O(^1D) + O_2(X)$, Can. J. Chem. 52 (1974) 4007–4015.

[16] L.C. Lee, T.G. Slanger, Observation on $O(^1D \rightarrow {}^3P)$ and $O_2(b^1\Sigma_g^+ \rightarrow X^3\Sigma_g^+)$ following O_2 photodissociation, J. Chem. Phys. 69 (1978) 4053–4060.

[17] T.G. Slanger, Vibrational excitation in $O_2(b^1\Sigma_g^+)$, Can. J. Phys. 64 (1986) 1657–1663.

[18] P.M. Borrell, P. Borrell, D.S. Richards, Q. Quinney, The quenching of the $O_2(b^1\Sigma_g^+)$ at high temperature, Faraday Tr. II 83 (1987) 2045–2052.

[19] U. Schurath, The energy pooling reaction $2O_2(a^1\Delta_g) \rightarrow O_2(X^3\Sigma_g^-) + O_2(b^1\Sigma_g^+)$: Formation, relaxation, and electronic quenching of vibrationally excited $O_2(b^1\Sigma_g^+)$, J. Photochem. 4 (1975) 215–226.

[20] J.G. Parker, Collisional deactivation of laser excited singlet molecular oxygen by ozone, J. Chem. Phys. 67 (1977) 5352–5361.

[21] H. Klingshirn, B. Faltermeier, W. Hengl, M. Maier, Non-exponential decay of the fluorescence from the $a^1\Delta_g$ state in liquid oxygen at high excitation intensities, Chem. Phys. Lett. 93 (1982) 485–489.

[22] E. Wild, H. Klingshirn, B. Faltermeier, M. Maier, Relaxation mechanism of the $a^1\Delta_g$ state of liquid O_2, Chem. Phys. Lett. 93 (1982) 490–494.

[23] O. Klais, A.H. Laufer, M.J. Kurylo, Atmospheric quenching of vibrationally excited $O_2(a^1\Delta_g)$, J. Chem. Phys. 73 (1980) 2696–2699.

[24] R.D. Kenner, E.A. Ogryzlo, P.T. Wassell, Excitation of the green line in the night airglow, Nature 291 (5814) (1981) 398–399.

[25] R.D. Kenner, E.A. Ogryzlo, Quenching of the $O_2(A_{v=2} \rightarrow X_{v=5})$ Herzberg I band by O_2(a) and O, Can. J. Phys. 62 (1984) 1599–1602.

[26] J. Wildt, G. Bednarek, E.H. Fink, Laser excitation of $O_2(b^1\Sigma_g^+, v=0,1,2)$-rates and channels of energy transfer and quenching, Chem. Phys. 122 (1988) 463–470.

[27] D.R. Bates, Oxygen band system transition arrays, Planet. Space Sci. 37 (1989) 831–837.

[28] E.S. Hwang, A. Bergman, R.A. Copeland, T.G. Slanger, Temperature dependence of the collisional removal of $O_2(b^1\Sigma_g^+, v=1$ and 2) at 110–260 K, and atmospheric applications, J. Chem. Phys. 110 (1999) 18–24.

[29] T.G. Slanger, R.A. Copeland, Energetic oxygen in the upper atmosphere and the laboratory, Chem. Rev. 103 (2003) 4731–4765.

[30] V.A. Yankovsky, Electron-vibrational relaxation of $O_2(b^1\Sigma_g^+, v=1,2)$ molecules in collision with ozone, oxygen molecules and atoms, Khim. Fiz. 10 (1991) 291–306. Russ. J. Phys. Chem. B; ISSN PRINT: 1990-7931: ISSN ONLINE: 1990-7923 (in Russian).

[31] H. Klingshirn, M. Maier, Quenching of the $^1\Sigma_g^+$ state in liquid isotopes, J. Chem. Phys. 82 (1985) 714–719.

[32] J. Hedin, J. Gumbel, J. Stegman, G. Witt, Use of O_2 airglow for calibrating direct atomic oxygen measurements from sounding rockets, Atmos. Meas. Tech. 2 (2009) 801–812.

[33] R.D. Sharma, A.T. Stair Jr., H.A. Smith, A space-borne passive infrared experiment for remote sensing of the atomic oxygen density and temperature, and total density in the upper atmosphere, Adv. Space Res. 7 (10) (1987) 31–38.

[34] K.U. Grossmann, M. Kaufmann, K. Vollmann, The fine structure emission of thermospheric atomic oxygen, Adv. Space Res. 19 (1997) 595–598.

[35] K.U. Grossmann, M. Kaufmann, E. Gerstner, A global measurement of lower thermosphere atomic oxygen densities, Geophys. Res. Lett. 27 (2000) 1387–1390.

[36] J.P. Russell, R.P. Lowe, Atomic oxygen profiles (80–94 km) derived from Wind Imaging Interferometer/Upper Atmospheric Research Satellite measurements of the hydroxyl airglow: 1. Validation of technique, J. Geophys. Res. 108 (D21) (2003) 4662, http://dx.doi.org/10.1029/2003JD003454.

[37] J.P. Russell, W.E. Ward, R.P. Lowe, R.G. Roble, G.G. Shepherd, B. Solheim, Atomic oxygen profiles (80 to 115 km) derived from Wind Imaging Interferometer/Upper Atmospheric Research Satellite measurements of the hydroxyl and green airglow: local time-latitude dependence, J. Geophys. Res. 110 (2005) D15305, http://dx.doi.org/10.1029/2004JD005570.

[38] J.-H. Yee, R. DeMajistre, F. Morgan, The $O_2(b^1\Sigma_g^+)$ dayglow emissions: application to middle and upper atmosphere remote sensing, Can. J. Phys. 90 (2012) 769–784.

[39] T.G. Slanger, Studies of ionospheric processes in the atmosphere and the laboratory characterising the ionosphere, in: Meeting Proceedings RTO-MP-IST-056, AC/323(IST-056)TP/40, Neuilly-sur-Seine, France: RTO, 2006.

[40] V.A. Yankovsky, R.O. Manuilova, A.O. Semenov, Possibility of ozone and atomic oxygen retrievals from measured intensities of the molecule $O_2(b^1\Sigma_g^+, v\leqslant 2)$ emissions in the mesosphere and lower thermosphere, in: 38th Annual European Meeting on Atmospheric Studies by Optical Methods, Siuntio, Finland, 22–26 August, 2011, <http://www.sgo.fi/38AM/talks/contrib/Yankovsky_Report_in_Finland_2011.pdf>.

[41] R.O. Manuilova, O.A. Gusev, A.A. Kutepov, T. von Clarmann, H. Oelhaf, G.P. Stiller, A. Wegner, M. Lopez-Puertas, F.J. Martin-Torres, G. Zaragoza, J.M. Flaud, Modelling of non-LTE limb spectra of IR ozone bands for the MIPAS space experiment, J. Quant. Spectrosc. Radiat. Transfer 59 (1998) 405–422.

[42] M.G. Mlynczak, S.C. Solomon, D.S. Zaras, An updated model for $O_2(a^1\Delta_g)$ concentrations in the mesosphere and lower mesosphere and implications for remote sensing of ozone at 1.27 μm, J. Geophys. Res. 98 (D10) (1993) 18639–18648.

[43] SORCE – Solar Radiation and Climate Experiment NASA Science Mission, 2003. <http://science.nasa.gov/missions/sorce/>.

[44] SABER cite V2.0, 2015. <http://saber.gats-inc.com/data.php>.

[45] G.M. Fikhtengolts, Differential and integral calculus (in Russian), vol. 1, Publishing house: PHYSMATHLIT, Moscow, 2001. 608 pages. ISBN: 5-9221-0156-0, 5-9221-0155-2. 5-9221-0436-5.

[46] S.P. Sander, R.R. Friedl, A.R. Ravishankara, D.M. Golden, C.E. Kolb, M.J. Kurylo, R. E. Huie, V.L. Orkin, M.J. Molina, G.K. Moortgat, B.J. Finlayson-Pitts, Chemical Kinetics and Photochemical Data for Use in Atmospheric Studies, JPL Publication 02–25, Evaluation Number 14, California Institute of Technology, Pasadena, California, 2003.

[47] T. von Clarmann, Smoothing error pitfalls, Atmos. Meas. Tech. 7 (2014) 3023–3034, http://dx.doi.org/10.5194/amt-7-3023-2014.

[48] L. Chen, H. Rabitz, D.B. Considine, C.H. Jackman, J.A. Shorter, Chemical reaction rate sensitivity and uncertainty in a two-dimensional middle atmospheric model, J. Geophys. Res. 102 (D13) (1997) 16201–16214.

[49] S.M. Newman, A.J. Orr-Ewing, D.A. Newnham, J. Ballard, Temperature and pressure dependence of line widths and integrated absorption intensities for the $O_2(a^1\Delta_g)$–$O_2(X^3\Sigma_g^-)$ (0,0) transition, J. Phys. Chem. 104A (42) (2000) 9467–9480.

[50] P.H. Krupenie, The spectrum of molecular oxygen, J. Phys. Chem. Ref. Data 1 (2) (1972) 423–521.

[51] D.A. Newnham, J. Ballard, Visible absorption cross sections and integrated absorption intensities of molecular oxygen (O_2 and O_4), J. Geophys. Res. 103 (D22) (1998) 28801–28815.

[52] R.R. Gamache, A. Goldman, L.S. Rothman, Improved spectral parameters for the three most abundant isotopomers of the oxygen molecule, J. Quant. Spectrosc. Radiat. Transfer 59 (3/5) (1998) 495–509.

[53] N. Jacquinet-Husson, L. Crepeau, R. Armante, C. Boutammine, A. Chedin, N.A. Scott, C. Crevoisier, V. Capelle, C. Boone, N. Poulet-Crovisier, A. Barbe, A. Campargue, Chris Benner, Y. Benilan, B. Bezard, V. Boudon, L.R. Brown, L. Coudert, The 2009 edition of the GEISA spectroscopic database, J. Quant. Spectrosc. Radiat. Transfer 112 (2011) 2395–2445.

[54] V.D. Galkin, The moment of electronic transition $b^1\Sigma_g^+, v=0 \rightarrow X^3\Sigma_g^+$ of oxygen band system, Opt. Spectrosc. 47 (1979) 266–269.

[55] J. Hedin, L. Megner, M. Khaplanov, J. Gumbel, J. Stegman, T. Slanger, G. Witt, Oxygen species and thermospheric airglow in the earth's sky (O-States): a

rocket project on the O_2 atmospheric band, in: 41 Annual European Meeting on Atmospheric Studies by Optical Methods, Stockholm, August 16–22, 2014.
[56] K.S. Kalogerakis, T.G. Slanger, E.A. Kendall, T.R. Pedersen, M.J. Kosch, B. Gustavsson, M.T. Rietveld, Remote oxygen sensing by ionospheric excitation (ROSIE), Ann. Geophys. 27 (2009) 2183–2189.
[57] D.A. Pejakovic, R.A. Copeland, T.G. Slanger, K.S. Kalogerakis, $O_2(b^1\Sigma_g^+, v = 0, 1)$ relative yields in $O(^1D) + O_2$ energy transfer, J. Chem. Phys. 141 (2014) 024303.
[58] M.A. Blitz, T.J. Dillon, D.E. Heard, M.J. Pilling, I.D. Trought, Laser induced fluorescence studies of the reactions of $O(^1D_2)$ with N_2, O_2, N_2O, CH_4, H_2, CO_2, Ar, Kr and n-C_4H_{10}, Phys. Chem. Chem. Phys. 6 (2004) 2162–2171.
[59] S. Hadj-Ziane, B. Held, P. Pignolet, R. Peyrous, C. Coste, Ozone generation in an oxygen-fed wire-to-cylinder ozoniser at atmospheric pressure, J. Phys. D: Appl. Phys. 25 (1992) 677–685.
[60] D.A. Pejakovic, Z. Campbell, K.S. Kalogerakis, R.A. Copeland, T.G. Slanger, Collisional relaxation of $O_2(X^3\Sigma_g^-, v = 1)$ and $O_2(a^1\Delta_g, v = 1)$ by atmospherically relevant species, J. Chem. Phys. 135 (2011) 094309, http://dx.doi.org/10.1063/1.3624378.
[61] I.D. Clark, R.P. Wayne, The reaction of $O_2(^1\Delta_g)$ with atomic nitrogen and with atomic oxygen, Chem. Phys. Lett. 6 (1969) 405–407.